OPEN ACCESS

Repository of the Max Delbrück Center for Molecular Medicine (MDC) in the Helmholtz Association

http://edoc.mdc-berlin.de/14873

Cytoskeletal components define protein location to membrane microdomains

Szymanski, W.G. and Zauber, H. and Erban, A. and Wu, X.N. and Schulze, W.X.

This is a copy of the original article.

This research was originally published in Molecular & Cellular Proteomics. Szymanski, W.G. and Zauber, H. and Erban, A. and Wu, X.N. and Schulze, W.X.. Cytoskeletal components define protein location to membrane microdomains.. *Mol Cell Proteomics*.September 2015; 14(9):2493-2509 © 2015 by the American Society for Biochemistry and Molecular Biology Inc.

Molecular & Cellular Proteomics
2015 SEP 01 ; 14(9): 2493-2509
Doi: 10.1074/mcp.M114.046904

American Society for Biochemistry and Molecular Biology

© 2015 by The American Society for Biochemistry and Molecular Biology, Inc.
This paper is available on line at http://www.mcponline.org

Cytoskeletal Components Define Protein Location to Membrane Microdomains*[S]

Witold G. Szymanski‡, Henrik Zauber§, Alexander Erban‡, Michal Gorka‡, Xu Na Wu‡, and Waltraud X. Schulze¶‖

The plasma membrane is an important compartment that undergoes dynamic changes in composition upon external or internal stimuli. The dynamic subcompartmentation of proteins in ordered low-density (DRM) and disordered high-density (DSM) membrane phases is hypothesized to require interactions with cytoskeletal components. Here, we systematically analyzed the effects of actin or tubulin disruption on the distribution of proteins between membrane density phases. We used a proteomic screen to identify candidate proteins with altered submembrane location, followed by biochemical or cell biological characterization in *Arabidopsis thaliana*. We found that several proteins, such as plasma membrane ATPases, receptor kinases, or remorins resulted in a differential distribution between membrane density phases upon cytoskeletal disruption. Moreover, in most cases, contrasting effects were observed: Disruption of actin filaments largely led to a redistribution of proteins from DRM to DSM membrane fractions while disruption of tubulins resulted in general depletion of proteins from the membranes. We conclude that actin filaments are necessary for dynamic movement of proteins between different membrane phases and that microtubules are not necessarily important for formation of microdomains as such, but rather they may control the protein amount present in the membrane phases. ***Molecular & Cellular Proteomics 14: 10.1074/mcp.M114.046904, 2493–2509, 2015.***

Living cells need borders and molecular compartments for biochemical reactions and storage of metabolites. The plasma membrane therefore is a prerequisite for the evolution of different life forms. It consists of a phospholipid bilayer into which proteins and special lipid species such as sterols, sphingolipids, and glycolipids are inserted. The first complex model of plasma membrane was proposed in 1972 by Jonathan Singer and Garth Nicolson (1), replacing the concept of the plasma membrane as a strict protein–lipid–protein sandwich that was generally accepted until then. In Singer and Nicolson's model, the cell membrane is a two-dimensionally oriented viscous solution in which the membrane constituents are orientated in the most thermodynamically favorable manner, hiding hydrophobic hydrocarbon chains inside the lipid bilayer and exposing polar and ionic groups to the aqueous phase. This fluid mosaic model also implied that membrane proteins as well as lipid components are distributed in a homogeneous lipid bilayer at long range, but they can form specific aggregates and phases at short range, which were also termed "lipid rafts" or membrane microdomains.

Over the past 30 years, it has become evident that the plasma membrane is not such a homogeneous structure as it was initially proposed. We now know that the lipid bilayer is asymmetric (2) and that the free diffusion of membrane proteins is restricted by their interactions with intracellular and extracellular components (3). More recently, Simons and Ikonen suggested that large ordered phases, enriched with cholesterol and sphingolipids, emerge within the plasma membrane and that they function as platforms for enrichment of certain proteins while excluding others (4). This current membrane model suggests that the mixture of sterols and polar lipids within the plasma membrane can appear in two distinct phases: liquid disordered (L_d) and liquid ordered (L_o) phase (5). In this view, the so-called membrane microdomains are considered to be part of the L_o phase. Based on work on model membranes, it is suggested that lateral segregation of components into L_d and L_o phases occurs spontaneously (6) with the self-associating properties between sterols and highly saturated hydrocarbon chains of phopsho- and sphingolipids as the main driving force (7). Additionally, it is suggested that also specific lipid-protein and protein-protein interactions are essential for the formations of membrane domains as well as for stabilization of smaller nanodomains which subsequently may cause formation of larger platforms. In contrast to the animal cells, in plants these membrane microdomains seem to be rather immobile (8), possibly due to their attachment to the outer cell wall. More recently, it became obvious that membrane microdomains within a single

From the ‡Max Planck Institute of Molecular Plant Physiology, 14476 Potsdam, Germany; §Max-Delbrück Center of Molecular Medicine, Robert-Rössle-Straβe 10, 13092 Berlin, Germany; ¶University of Hohenheim, Department of Plant Systems Biology, 70593 Stuttgart, Germany

Received November 28, 2014, and in revised form, March 2, 2015
Published June 19, 2015, MCP Papers in Press, DOI 10.1074/mcp.M114.046904

Author contributions: H.Z. and W.X.S. designed research; W.G.S., A.E., M.G., and X.N.W. performed the research; X.N.W. contributed new reagents or analytic tools; W.G.S., H.Z., A.E., and W.X.S. analyzed the data; and W.G.S. and W.X.S. wrote the paper.

cell are highly diverse and of different compositions (9). Generally, in the plant model, organisms' plasma membrane microdomains turned out to be important in plant defense (10, 11), cell polarity (12, 13), and general signaling properties of the plasma membrane (14, 15).

The cytoskeleton was identified as an essential cellular component with important roles in membrane topography, bordering, trafficking, and organelle movement (16). Single particle tracking in mammalian cells revealed that the transferrin receptor and macroglobulin receptor demonstrate normal Brownian diffusion but only within a specific membrane compartment (17). Two hypothetical models were proposed in order to explain this phenomenon (supplemental Fig. 1). Direct interactions between transmembrane proteins and cytoskeleton are suggested to creates a barrier, called "fence," where cytosolic parts of transmembrane proteins collides with cytoskeletal components, limiting their diffusion to certain areas. These molecules can jump over the "fence" to a neighboring compartment, possibly due to the dynamic nature of the interaction of membrane proteins and cytoskeleton, where they are again temporally trapped (17). This phenomenon was recently described also in *A. thaliana* where the interplay between membrane microdomains and microtubules plays a role in secondary cell wall formation (reviewed in (18)). The second model assumes, additionally, that particular transmembrane proteins are anchored to and lined up along cytoskeleton and act as "pickets" to arrest free diffusion of other membrane components, including nontransmembrane proteins, within the enclosed compartment (19).

For plants, the composition of these sterol-rich membranes phases was analyzed in several biochemical studies (14, 20–22). Thereby, low-density preparations of plasma membrane fractions after treatment with nonionic detergents (DRM[1] fractions) were considered as a biochemical representation enriched in cellular membrane ordered phases or microdomains. Proteomic studies in mammalian cells consistently reported that the DRM fraction is highly enriched with several cytoskeletal proteins such as actin, tubulin, myosin, dynamin, actinin, and supervillin (23–25). Additionally, the level of phosphatidylinositol 4,5-bisphosphate (PI(4,5)P2), a lipid connecting the plasma membrane to actin filaments, was also significantly elevated in DRM preparations (26). Treatment with microtubule and actin depolymerizing agent results in drastic loss of many signaling proteins from these DRM fractions prepared from adult rat cardiac myocytes (27) or human embryonic retinal cells (28).

Based on this knowledge, we propose two hypothetical models for the relationship between cytoskeleton and membrane microdomains for plant cells: (i) Actin filaments and microtubules could be important in the membrane phase separation or formation of the membrane microdomains themselves. In this case, disruption of the cytoskeleton would cause a lack of phase segregation in the plasma membrane. (ii) The cytoskeleton is only important for the incorporation of specific protein into the sterol-enriched regions but not for the general formation of these phase separations. This view implies that phase separations or membrane microdomains would still be present after cytoskeleton disruption but their protein composition can be different. Another possible scenario is (iii) that cytoskeletal elements serve as anchors for membrane microdomains at particular position in the plasma membrane, so the absence of these anchors would cause the increased mobility of microdomains (supplemental Fig. 1).

The primary aim of this study was to characterize the interplay between cytoskeletal components and different membrane phases (microdomains) in *A. thaliana* suspension cell cultures. To reach this goal, biochemical and proteomic approaches were combined with confocal microscopy and activity assays measuring the influence of actin or tubulin disruption on the composition, localization, and biochemical properties of the sterol-enriched membrane microdomains. Thereby, for biochemical analyses, low-density detergent-resistant membrane fractions are analyzed as containing cellular sterol-rich membrane compartments.

MATERIALS AND METHODS

Plant Lines Expressing Proteins Fused to GFP/YFP/RFP—Seeds of an *A. thaliana* complementation line with YFP-tagged (yellow fluorescent protein) remorin 1.2 based on SALK line 117637 were obtained as a courtesy of Dr. Thomas Ott from Ludwig Maximilian University of Munich, Germany. Homozygous lines of *A. thaliana* expressing GFP-tagged leucin-rich repeat receptor-like kinase (LRR-RLK) At3G02880.1 under ^{35}S promoter were obtained as a courtesy from Xuna Wu, University of Hohenheim, Germany.

Seeds of an *A. thaliana* dual-labeled line for actin and tubulin were obtained as a courtesy of AG Persson from the Max Planck Institute of Molecular Plant Physiology in Golm, Germany. This line allowed observation of the structure of microtubules and actin filaments in the same plant at the same time. The dual-labeled line was created by transformation of Col-0 with pART27 vector containing GFP-FABD2 fusion construct under ^{35}S promoter together with a gene for kanamycin resistance (29). This line was subsequently crossed with another line that was transformed with a Gateway vector containing TUA5 fused to mCherry-RFP under ^{35}S promoter together with genes for kanamycin resistance (30).

Seedlings—Sterilized seeds of YFP-tagged remorin lines were grown on 1/2 Murashige–Skoog medium containing 1.5% agarose, 1% sucrose, and kanamycin. Seedlings transferred on plates were left for 5 days in a light-dark cycle with a 16-h photoperiod at 23 °C. Prior to the performed experiments, seedlings were carefully moved into the cavity of a six-well plate filled with 1/2 liquid MS medium with 1% sucrose and placed on a rotary shaker (50 rpm).

Cell Suspension Cultures—Cell suspension cultures were established from *A. thaliana* Col-0 leaf callus as described (31). They were grown in flasks in full JPL medium under constant light conditions at 80–100 mol $m^{-2}s^{-1}$ at 23 °C with rotary shaking at 120 rpm. Cells were subcultured every 7 days. In order to perform experiments, cell cultures were pooled from and independent flask and subsequently divided into desired numbers of replicates for treatment. In general,

[1] The abbreviations used are: DRM, detergent-resistant membrane fraction; DSM, detergent-soluble membrane fraction; ER, endoplasmic reticulum; PM, plasma membrane.

ASBMB MOLECULAR & CELLULAR PROTEOMICS MCP

treatment experiments were carried out in at least three biological replicates, and results are presented as an average of these.

Treatment with Cytoskeleton Depolymerizing Agents—Experiments were performed with cytochalasin D, which is a potent inhibitor of actin polymerization. Cytochalasin D binds to G-actin and prevents polymerization of actin monomers (32), as well as to the barbed end of actin filaments, which inhibits the association of hew monomers at that end (33). The second drug used in the experiments was oryzalin (3,5-dinitro-N4, N4-dipropylsulfanilimide), which is a selective pre-emergence, surface-applied dinitroaniline herbicide with rather low toxicity to animals and fungi. This drug acts as a microtubule depolymerizing agent, and it perturbs all microtubule-related processes in plant cells (34, 35). Both inhibitory effects were shown to be reversible (36). Stock solutions of cytochalasin D and oryzalin were dissolved in DMSO. The following experimental conditions were applied:

Cytochalasin D treatment: Cells treated with cytochalasin D may react to the loss of the links between the plasma membrane and actin filaments by creating more filaments that might compensate for the initial depolymerizing effect of cytochalasin D (37). In order to evaluate this effect, time points instead of different concentrations were used. Cell cultures were treated with cytochalasin D in concentration of 500 nM for different periods: 30 min, 60 min, 90 min, and 120 min. The concentration used was far lower than the minimal concentration known to disrupt cytoplasmic streaming (38). Control samples were treated with respective volumes of DMSO solution. The concentration of DMSO in final solutions was not higher than 0.1%. After treatment, cells were filtered and immediately frozen in liquid nitrogen.

Oryzalin treatment: According to the literature, oryzalin has an impact on the normal structure of the microtubules already at nanomolar concentrations but often requiring long exposure (34, 35). In order to perform experiments at similar time frames as the cytochalasin D treatment, we selected increasing oryzalin concentrations applied for the duration of 1 h. Cell cultures were treated with different concentrations of oryzalin (1 μM, 2 μM, 5 μM, and 10 μM) for 1 h. Instead of a disrupting agent, respective amount of DMSO was added to control samples. The concentration of DMSO in final solutions was not higher than 0.1%. After treatment, cells were filtered and immediately frozen in liquid nitrogen.

Enzyme Activity Measurements—Activity of the plasma membrane H^+-ATPase in DRM and DSM fractions was measured by the malachite green colorimetric assay (39). The standardization of different samples was based on total protein content, which was evaluated by the NanoOrange Protein Quantitation Kit (Invitrogen, Germany) according to the instructions. Specific inhibitors of P-type and V-type ATPases were used to distinguish the specific activity of selected enzyme from the background activity of the sample: Na_3VO_4 as plasma membrane ATPase inhibitor, EDTA as inhibition of Ca^{2+}-ATPases, NaN_3 as inhibition of mitochondrial ATPases, and bafilomycin A1 as inhibitor of V-ATPases (40).

In order to perform enzymatic activity measurement, 1 μg of extracted protein was used per reaction mixture. The plate was placed on a shaker at 37 °C. Reaction was stopped after 1 or 2 h by adding MG-AM-TRIT [three volumes of MG solution (2 mM malachite green in Milipore water) and one volume of AM solution (0.034 M ammonium molybdate in 4 N HCl, 0.1% Triton X-100) solution to each well. Addition of sodium citrate to a final concentration of 3% inhibited the color development. The change in phosphate concentration was measured by absorption using the wavelength of 630 nm.

Preparation of Membrane Fractions for Proteomic Analysis—In general, microsomal fractions, plasma membrane, and DRM/DSF fractions were prepared as described in detail (41). Frozen plant material was powderized, mixed with two volumes of extraction buffer (100 mM Hepes-KOH (pH 7.5); 250 mM sucrose; 10% (w/v) glycerol; 5 mM EDTA; 5 mM ascorbic acid; 0.6% (w/v) PVP K-25; freshly added:

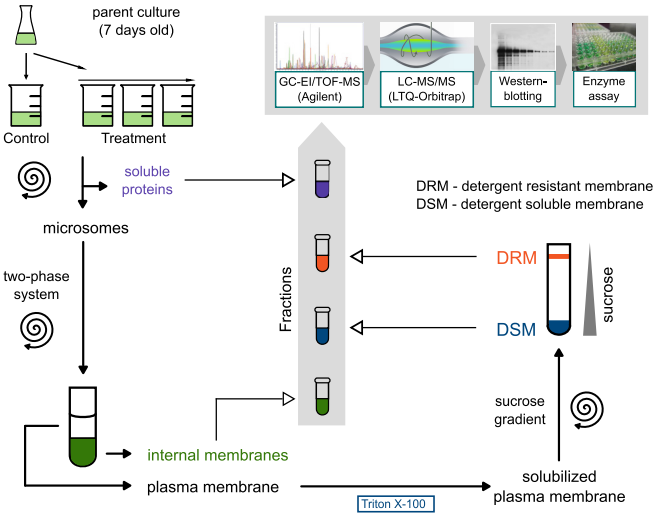

FIG. 1. **Protein fractionation and analysis scheme.** During isolation of DRM other protein fractions were collected, including soluble proteins, internal membranes, and DSM, which were all subsequently analyzed by a combination of different biochemical and mass spectrometry methods.

5 mM DTT; 1 mM PMSF; protease inhibitor mixture (SIGMA, Germany)), and stirred gently on ice until complete homogenization was achieved. The homogenate was then filtered through one layer of Miracloth (Merck, Germany), and cell debris was spun down at 10,000 g for 8 min. The supernatant was taken and centrifuged at 100,000 g for 30 min. After this step, microsomes were acquired in the pellet and soluble proteins (SOL fraction) in supernatant (Fig. 1). The microsomal fraction was solubilized in resuspension buffer (5 mM potassium phosphate; 0.33 M sucrose; 3 mM KCl; 0.1 mM EDTA; freshly added: 1 mM DTT, 1 mM PMSF) and then deposited onto a two-phase system of polyethyleneglycol and dextran (41). After gentle mixing and centrifugation at 1,000 g for 10 min, the lower green phase contained intracellular membranes (IM fraction) while the upper phase contained cell plasma membrane (PM fraction). The latter was collected, diluted with five volumes of resuspension buffer and centrifuged again at 200,000 g for 1 h. The obtained pellet was then resuspended in TNE buffer (25 mM Tris-HCl pH 7.5; 150 mM NaCl; 5 mM EDTA; 1 mM DTT), and protein concentration was measured using Bradford assay (42). At this step, an aliquot of the plasma membrane protein was taken for analysis (Fig. 1).

Solubilized in TNE buffer, the plasma membrane was subsequently treated with Triton X-100 in a concentration between 0.5 and 1% and in a ratio of proteins to Triton of 1:15. The detergent treatment was applied for 30 min on ice with shaking. Detergent-resistant and detergent-soluble membranes created after Triton X-100 were separated by centrifugation for 18 h through a sucrose step gradient (from the bottom: 1.8 M, 1.6 M, 1.4 M, 0.15 M). After centrifugation, a low-density band was observed as a white ring at the interface of the 0.15 M and 1.4 M sucrose phases (41). A fraction of 1 ml containing the ring was collected as DRM fraction, and 1 ml from the bottom of the gradient was collected as DSM fraction.

Recovery of Proteins from the Sucrose Gradient—For mass spectrometry: Proteins from collected fractions were purified by methanol-chloroform method. Initially, four volumes of methanol, one volume of chloroform, and three volumes of water were added to the sample, and after each addition, the sample was vortexed. Next, the sample was centrifuged for 15 min at room temperature. The upper phase was removed, and the lower phase was diluted with three volumes of

methanol. Protein was then pelleted by centrifugation for 15 min at maximum speed (20,800 g).

For enzymatic measurements: The recovery of proteins from collected sucrose gradient fractions was based on dissolving the dense sucrose with large volumes of buffer TNE and subsequently pelleting membranes by ultracentrifugation at 200,000 g for 1 h.

In Solution Protein Digestion and Desalting—Purified proteins from preceding steps were dissolved in 6 M urea/2 M thiourea, pH 8, which causes denaturation of proteins. Subsequently, disulfide bonds were released by treatment with DTT, and spontaneous oxidation was prevented by carbamidomethylation with iodoacetamide. Lys-C and trypsin were applied for the digestion of proteins and creation of low-molecular-weight tryptic peptides as described (41). After trypsin digestion, samples were desalted on C18 Stop And Go Extraction tips (C18 Empore Disks, 3 M) (43), dried in a vacuum concentrator, and resuspended in 1% trifluoroacetic acid, 5% acetonitrile just before loading onto the liquid chromatography column.

LC-MS/MS Analysis of Peptides—Digested and desalted peptides were analyzed by LC/MS/MS using nanoflow HPLC (Easy nLC, Thermo Scientific) and an Orbitrap hybrid mass spectrometer (LTQ-Orbitrap XL, Thermo Scientific) as mass analyzer. Peptides were eluted from a 15 cm long, 75 m wide analytical column filled with C18 beads (Reprosil C18, Dr. Maisch GmbH, Germany) on a linear gradient running from 5% to 80% acetonitrile in 90 min at a flow rate of 250 nl/min and sprayed directly into the mass spectrometer. Proteins were identified by tandem mass spectrometry (MS/MS) by information-dependent acquisition of fragmentation spectra of multiple-charged peptides. Up to five data-dependent MS/MS spectra were acquired in the linear ion trap for each FTMS full scan spectrum acquired at 60,000 full-width half-maximum resolution settings with an overall cycle time of 1 s.

For raw file peak extraction and protein identification, we used MaxQuant software (44) (version 1.4.2.1) with *A. thaliana* TAIR10 protein sequences (35,386 entries) used by the search engine Andromeda (45). The following additional parameters were applied: trypsin as cleaving enzyme; 10 ppm peptide mass tolerance; 0.8 Da MS/MS tolerance; maximal two missed cleavages allowed, threshold for validation of peptides set to 0.01 using a decoy database, acetylation at N-terminal of proteins, and oxidation of methionine set as variable modification, carbamidomethylation of cysteine set as a fixed modification, "label-free quantification" marked, "match between runs" marked, minimum peptide length of six amino acids, and retention time correlation enabled (time window of 2 min). Spectra of identified peptides are available in supplemental Fig. 2. Known contaminants, such as keratins, were excluded from further analysis.

Label-Free Protein Intensities Calculation—Peptide lists derived from MaxQuant (evidence.txt) were processed by an R-based script (cRacker (46)) allowing for automated and standardized processing. Peptides with the assigned MaxQuant score below 30 and peptides that were quantified in less than 90% of all fraction-specific samples were filtered out. The principal steps of the normalization and quantitation were: (i) All peptide intensities within each sample were normalized to fraction of total ion-intensity sums. (ii) To compensate effects of normalization due to the number of detected peptides per sample, intensity was proportionally corrected to the reciprocal number of identified peptides in each sample using the integrated normalization option in cRacker. (iii) Peptide intensities with missing values in more than the permitted numbers of samples within replicates of each fraction were filtered out. (iv) Outliers exclusion was used to lower the influence of extreme peptide intensity values on the average protein intensity. (v) Remaining normalized peptide intensities were z-score scaled and mean averaged.

Protein Gel Blots—Protein concentration in different fractions after chloroform/methanol extraction was evaluated by NanoOrange (Invitrogen) according to the instructions and equal amounts of proteins (10 μg) per sample were loaded onto 10% polyacrylamide gels. SDS-polyacrylamide gel electrophoresis and protein gel blots were performed as described (47). The membrane was blocked in blocking solution overnight at 4 °C and was subsequently washed three times with PBS-T (0.2% Tween-20, 10 mM NaCl, 2.7 mM KCl, 10 mM Na_2HPO_4, and 2 mM KH_2PO_4, pH 7.4) and later incubated with the primary antibody αGFP at the concentration of 1:10,000 in PBS-T for 1 h at room temperature. After additional washing steps, the secondary antibody alkaline phosphatase coupled anti-mouse IgG was used at the concentration of 1:10,000 in PBS-T for 1 h at room temperature. For detection of the signal, blots were incubated in alkaline phosphatase-detection buffer (pH 9.5) with addition of 5-bromo-4-chloro-3′-indolyphosphate p-toluidine salt and nitro-blue tetrazolium chloride.

Extraction of Lipids—After density gradient centrifugation for the separation of DRM and DSM, a volume of 1 ml for the low-density band (DRM) as well as 1 ml from the bottom of the gradient (DSM) was transferred to the clean 15 ml falcon tube. For each 1 ml of sample, 5 μl of 5 mM 3-hydroxy-5-cholestane (cholestanol) was added, which reflected 10 μg of this compound and served as an internal standard. Lipids were extracted by the chloroform-methanol method (48). To each sample 3.75 ml of 1:2 (v/v) $CHCl_3$:CH_3OH were added, then 1.25 ml of $CHCl_3$, and finally 1.25 ml of water. Tubes were vortexed thoroughly after each solvent addition. The final mixture was centrifuged at 200 g for 5 min at room temperature, which resulted in a separation into upper aqueous and bottom organic phases. The aqueous solution was removed using a Pasteur pipette, and the organic phase was washed with "authentic upper phase" (prepared by performing blank chloroform-methanol extraction on water). The cleaned organic phase was subsequently transferred in batches of 500 μl to a smaller tube and dried in a vacuum concentrator. By repeatedly drying down small volumes, the spread of extracted lipids around the whole inner surface of the tube was minimized.

Metabolite Profiling—The profiling of soluble metabolites was performed as described previously (49) by gas chromatography coupled to electron impact ionization/time-of-flight mass spectrometry (GC-EI/TOF-MS). Dried lipid species were methoxyaminated and trimethylsilylated manually prior to GC-EI/TOF-MS analysis. Analysis was performed using an Agilent 6890N24 gas chromatograph (Agilent Technologies, Boeblingen, Germany) with splitless injection onto a FactorFour VF-5ms capillary column, 30 m length, 0.25 mm inner diameter, 0.25 m film thickness (Varian-Agilent Technologies) connected to a Pegasus III time-of-flight mass spectrometer (LECO Instrumente GmbH, Moenchengladbach, Germany). Retention indices were calibrated by addition of a C_{10}, C_{12}, C_{15}, C_{18}, C_{19}, C_{22}, C_{28}, C_{32}, and C_{36} n-alkane mixture to each sample (50).

GC-EI/TOF-MS chromatograms were acquired, visually controlled, baseline corrected, and exported in NetCDF file format using ChromaTOF software (Version 4.22; LECO, St. Joseph, MI). GC-MS data processing into a standardized numerical data matrix and compound identification were performed using the TagFinder software (51, 52). Compounds were identified by mass spectral and retention time index matching to the reference collection of the Golm metabolome database (http://gmd.mpimpgolm.mpg.de/) (53–55). Guidelines for manually supervised metabolite identification were the presence of at least three specific mass fragments per compound and a retention index deviation within 1.0%. All mass features of an experiment were normalized by sample fresh weight, internal standard (C_{22}), and were then maximum scaled.

Confocal Microscopy—Fluorescence imaging shown in the study was performed as described below. The fluorescent signal of GFP, YFP, and mCherry was recorded using Leica TCS-SP2 system coupled with DM6000 inverted light microscope and HCX PL APO 63.0 × 1.20 W CORR objective. The excitation was achieved using 488 nm

ASBMB MOLECULAR & CELLULAR PROTEOMICS MCP

argon laser for GFP, 514 nm argon laser for YFP, and 561 nm diode laser for mCherry. Resulting emission was separated using triple dichroic TD 488/543/633 for GFP, dichroic RSP 500 for YFP, and double dichroic DD488/543 for mCherry. Separated light was collected and amplified using PMT detectors between 502–550 nm for GFP, 505–550 for YFP, and 577–650 nm for mCherry. Images were acquired with resolution of 1,024 × 1,024 pixels. Pinhole was set between 0.295 and 1 Airy unit.

Statistical Analyses and Data Visualization—All statistical tests on proteomic data, such as hierarchical clustering and k-means clustering, were automated and performed by the R-based script cRacker (46). Information on subcellular location was taken from SUBA3 (56), and functional annotation was done according to MAPMAN (57). ANOVA analysis was used to test for significant differences between quantitative values on the protein level in the various samples and treatments. Differences with the p value $< .05$ in comparison to the control samples were taken as significant. Statistical assessments on sterol and metabolite data, such as hierarchical cluster analysis, heat map, and other data visualizations, were performed with the multiexperiment viewer software MeV (Version 4.6.2) (58, 59).

RESULTS

The aim of this study was to characterize effects of cytoskeletal disruption on protein distribution between low-density sterol-rich microdomains (as biochemically extracted in the form of DRM) and general other higher-density membrane phases (DSM).

Cytoskeletal Disruption Does Not Affect Sterol Content of the Membrane—Two major phytosterols, sitosterol and campesterol, were identified and quantified in DRM and DSM fractions, with generally higher values in DRM fractions. Generally, these sterols contribute to about 20% of the plasma membrane lipids. No other typical membrane sterols were identified but rather organic acids, sugars, alkanes, and many unidentified compounds containing an alkyl group were characterized in the GC-TOF analysis. In both fractions, a variety of soluble compounds like ethyl-hexanoic acid, hydroxy-pyridine, octadecane, diethylene glycol, boric acid, or phosphoric acid were detected (Fig. 2*A*). These other compounds may have masked the detection of other lower abundant lipids. Most of these substances, except for ethanolamine, were considered as copurifying contaminants since they were not known to be membrane components.

The cytoskeletal disruption did not result in statistically significant relative and absolute changes in any of the identified substances. Both sterols grouped in the same hierarchical cluster of compounds. The level of sterols in DRM as well as in DSM fractions remained unaltered in response to cytochalasin D and oryzalin treatment, and as expected, sterol levels were higher on average in DRM fractions (Fig. 2*B*). Thus, we conclude that disruption of actin filaments or disruption of microtubules does not cause a drastic change in membrane sterol composition.

General Proteomic Comparison of Collected Fractions—Detergent-resistant membrane preparations are prone to copurifying nonsterol-dependent proteins and may be considered an enrichment but not a purification of sterol-rich membrane microdomains (60). In order to robustly establish a filter for identification of true effects of cytoskeletal disruption on changes in protein distribution between cellular membrane phases, reference protein lists of know sterol-dependent proteins, as well as from intracellular membrane proteins and soluble proteins, were established (60). In the cytochalasin D experimental series, 557 proteins were identified in DRM fractions (five replicates), a total of 918 proteins were identified in DSM fractions (four replicates), and 588 and 1,558 proteins were identified from intracellular membranes (IM, two replicates) and as soluble proteins (SOL, four replicates). For oryzalin treatment experiments, 449 proteins were identified in detergent-resistant membranes (five replicates), 996 proteins in detergent-soluble membranes (five replicates), 1,313 proteins in intracellular membranes (four replicates), and 776 proteins as soluble proteins from two biological replicates (supplemental Fig. 2*A*). Separation quality of cellular fractions was confirmed by the fact that in almost all fractions collected, a large number of proteins was identified in a single fraction only (unique proteins). The largest overlap between collected fractions was represented by the proteins from neighboring compartments, for example, 154 or 204 proteins overlapping between DRM and DSM fractions while only 37 or one protein was in common for detergent-resistant membranes and soluble fraction (supplemental Fig. 3*A*).

The identified proteins were then assigned to expected cellular location based on SUBA3 (56). As expected, in both drug treatment series, the majority of proteins identified in the DRM fraction had a plasma membrane location, while proteins identified in the IM fraction largely were of mitochondrial, plastidial, and endoplasmic reticulum location. The SOL fraction contained the highest amount of soluble proteins (supplemental Fig. 3*B*). Furthermore, filtering out all proteins that were found in more than one fraction enriched the fraction-specific protein groups at an even higher degree (unique proteins in supplemental Fig. 3*B*). In further analyses, proteins were excluded if their abundance was highest in IM or SOL fractions, even when detected in DRM or DSF fractions. This filtering procedure was validated in detail in a previous study (60).

Effects of Cytoskeletal Disruption on Membrane Protein Distributions—To confirm the specificity of cytochalasin D and oryzalin treatment on the disruption of actin filaments and tubulins, respectively, the disappearance of actin or tubulin protein in the DRM fraction was monitored (Fig. 3*A*). Cytochalasin D treatment depleted the sample from ACT3 within 30 min of treatment, but a less strong effect was observed for ACT2. Oryzalin treatment efficiently depleted different tubulin isoforms from the DRM fraction in a concentration-dependent manner.

Secondly, specificity of the drug treatment was monitored using the dual-labeled line for actin and tubulin (Fig. 3*B*). Cytochalasin D treatment of 1 h was already enough to significantly disrupt the majority of actin filaments, but some

ASBMB MOLECULAR & CELLULAR PROTEOMICS MCP

ASBMB
MOLECULAR & CELLULAR PROTEOMICS
MCP

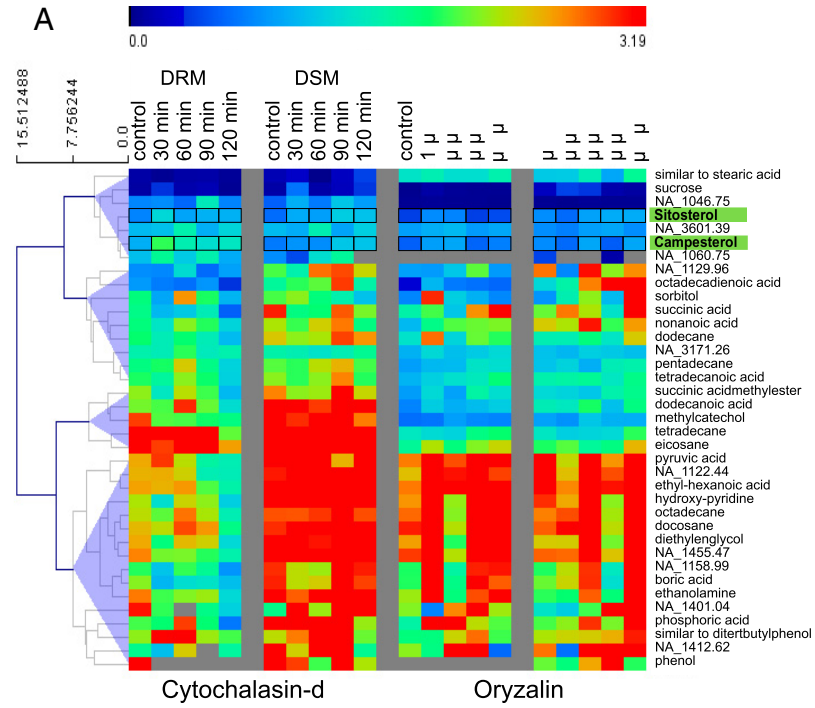

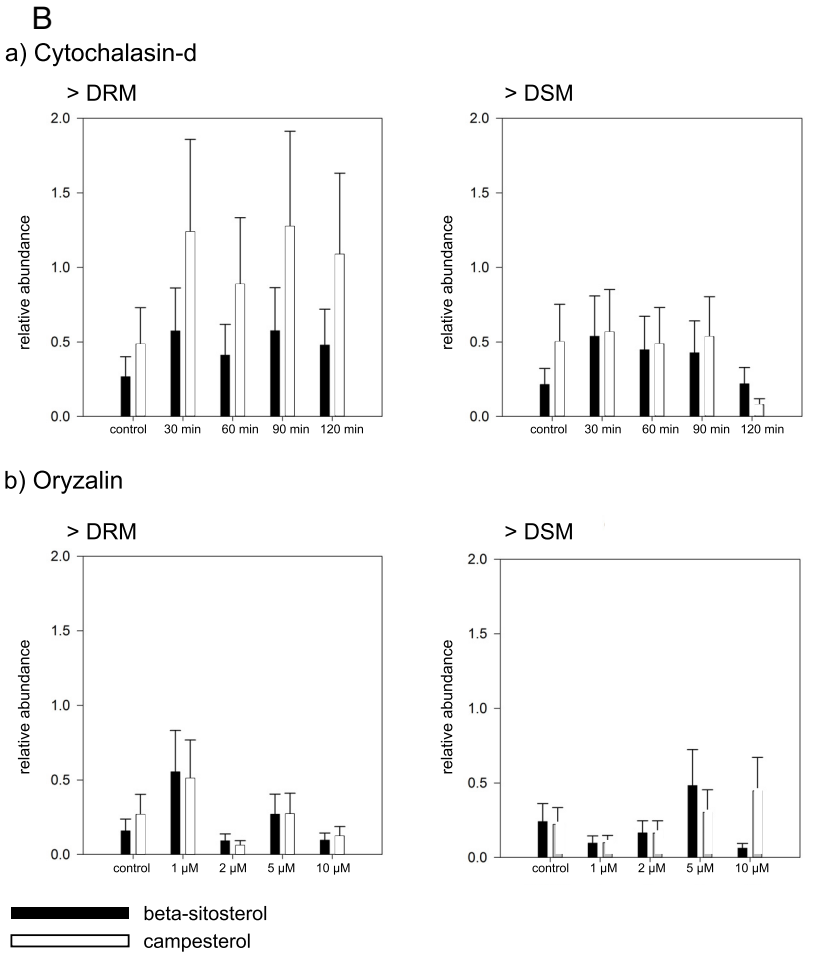

actin strands still remained visible. Microtubule structures were not affected by the cytochalasin D treatment. Oryzalin treatment at a concentration of 5 μM for 1 h completely disintegrated typical microtubule structures, while actin filaments remained intact. Thus, the drug treatments applied in our experiments specifically affected only one component of the cytoskeleton.

Cluster analysis of the abundance profiles of DRM proteins in response to cytochalasin D time course treatment revealed five major response groups (supplemental Fig. 4*A*). The largest number of proteins (199 proteins) was found in cluster 3, with a tendency for an increase of abundance in response to the treatment. However, these were mainly cytosolic proteins (66%) and very few plasma membrane proteins (6%). The cluster with the highest fraction of plasma membrane proteins (46%) was cluster 1 (144 proteins), with a tendency of decreased abundance in the DRM fraction. Clusters with a high content of cytosolic proteins (clusters 2 and 3) particularly contained proteins involved in protein synthesis (ribosomal proteins). Such proteins are known copurifying proteins in DRM preparations (60). In contrast, clusters 1, 4, and 5, with high fraction of membrane proteins particularly, were rich in proteins with transport and signaling functions (these functions made up 18 and 15% of all proteins in cluster 1).

Similarly, oryzalin treatment over the range of concentrations resulted in differential responses of proteins, which could be separated into five response clusters (supplemental Fig. 4*B*) containing 51 (cluster 4) to 113 proteins (cluster 2). Proteins in cluster 1 showed an increased abundance with increased concentration of oryzalin, but these were particularly proteins with cytosolic location such as ribosomal proteins. Proteins in two clusters with a high fraction of membrane proteins (62% in cluster 2 and 67% in cluster 4) displayed a decreased abundance profile in DRM with increasing oryzalin concentration but at different slope. These clusters were particularly enriched in proteins with signaling function (3% in cluster 2) or transporters (40% in cluster 4).

However, cytochalasin D or oryzalin treatment of cell cultures did not affect global protein abundance levels and distribution of proteins identified in the IM and SOL fractions (supplemental Fig. 5). These findings suggest that the observed drug-induced protein abundance changes for proteins identified in DRM and DSM fractions were mainly due to local redistributions within the membrane and not due to global redistributions between compartments based on disturbed membrane trafficking.

In order to identify candidate DRM proteins significantly affected by the cytoskeletal disruptions, three filtering criteria were applied to the above data set: (i) proteins were required to be identified in DRM fractions in at least one replicate of this study, (ii) proteins were required to show significant response to drug treatment (ANOVA p value cutoff .05 after multiple testing (61)), and (iii) have evidence for sterol-dependent membrane location from previous work (22, 60, 62). Based on these criteria, for cytochalasin D treatment, from the 557 proteins identified in DRM fractions, only 50 proteins had previously been confirmed also as sterol-dependent proteins (Fig. 4). For oryzalin treatment, out of 449 proteins identified in DRM fractions, 66 proteins were also characterized as sterol-dependent. From this overlap, 22 proteins were found to significantly display an altered abundance distribution between DRM and DSF upon cytochalasin D treatment, and 13 proteins were found to significantly change their distribution profile in response to oryzalin. In most cases, cytoskeleton disruption, particularly treatment with cytochalasin D, induced a reduced abundance of proteins in sterol-enriched DRM fractions with an accompanied increased abundance of that protein in the sterol-depleted DSM fraction (DRM/DSM ratios in Table I). This may indicate that these proteins within the membrane moved from sterol-enriched phases into sterol-depleted membrane phases, particularly after disruption of actin filaments.

Out of the 22 proteins with significantly altered distribution between DRM and DSM upon cytochalasin D treatment (Table I; supplemental Fig. 6*A*), there were eight proteins involved in membrane transport, four signaling proteins, two oxidases, two proteins with functions in stress responses, a remorin protein, and few others with unassigned functions. Among the 13 proteins with significant response to oryzalin, we found seven transporters, three signaling proteins, a remorin, one protein involved in abiotic stress responses, and one protein with unspecified role in plant development (Table I; supplemental Fig. 6*B*). Among all these proteins, nine proteins showed altered distribution between DRM and DSM upon both treatments, namely disruption of actin filaments as well as upon disruption of microtubules (supplemental Fig. 7). Thereby, six proteins (AHA1, AHA2, ERD4, RLK902, AT3G61260, AT3G02880) were depleted from DRM in both drugs, one protein (PATL1) increased in DRM fractions upon both drugs, and two proteins (AVP1 and VHA-A3) showed opposite behavior upon actin or microtubule disruption.

Fig. 2. (*A*) Changes of the level of all identified compounds in GC-MS analysis. Raw intensities obtained by the mass analyzer were normalized to the internal standard (3′-hydroxy-,5′-cholestane) that was spiked to every sample before sterol extraction. Intensities of the β-sitosterol and campesterol are highlighted with black squares. (*B*) Changes of the level of identified sterols in response to applied treatments. Barplots represent intensities normalized to the internal standard that was used (3′-hydroxy-,5′-cholestane). No significant changes (ANOVA, $p < .05$) in measured sterol levels after (*a*) cytochalasin D and (*b*) oryzalin treatment were observed in DRM and DSM fractions. Cytochalasin D in concentration of 500 nM for 30, 60, 90, and 120 min was applied to cell cultures. Oryzalin was applied to cell cultures for 1 h in increasing concentration range of 1 μM, 2 μM, 5 μM, and 10 μM.

ASBMB MOLECULAR & CELLULAR PROTEOMICS MCP

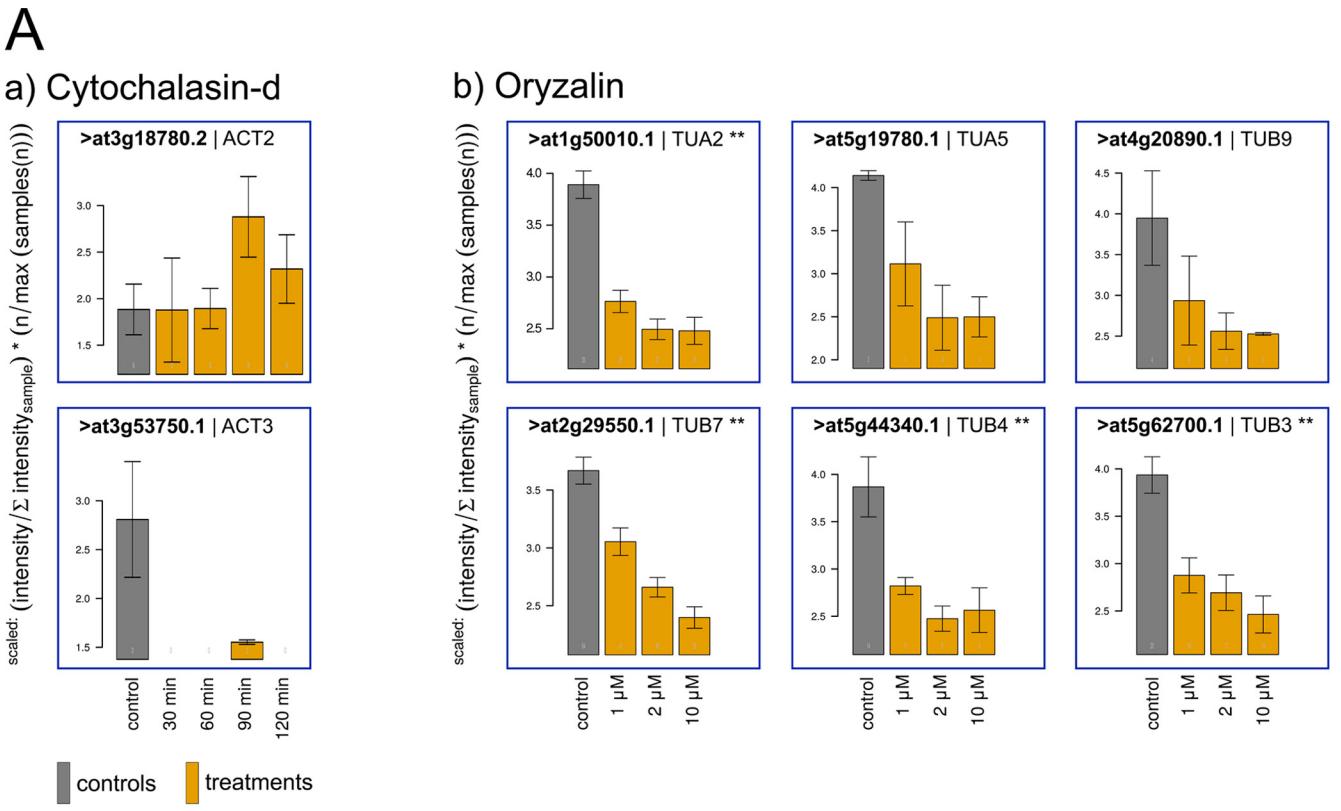
A
a) Cytochalasin-d
b) Oryzalin
scaled: (intensity/Σ intensity_sample) * (n/max (samples(n)))
>at3g18780.2 | ACT2
>at3g53750.1 | ACT3
>at1g50010.1 | TUA2 **
>at5g19780.1 | TUA5
>at4g20890.1 | TUB9
>at2g29550.1 | TUB7 **
>at5g44340.1 | TUB4 **
>at5g62700.1 | TUB3 **
control
30 min
60 min
90 min
120 min
1 µM
2 µM
10 µM
controls
treatments

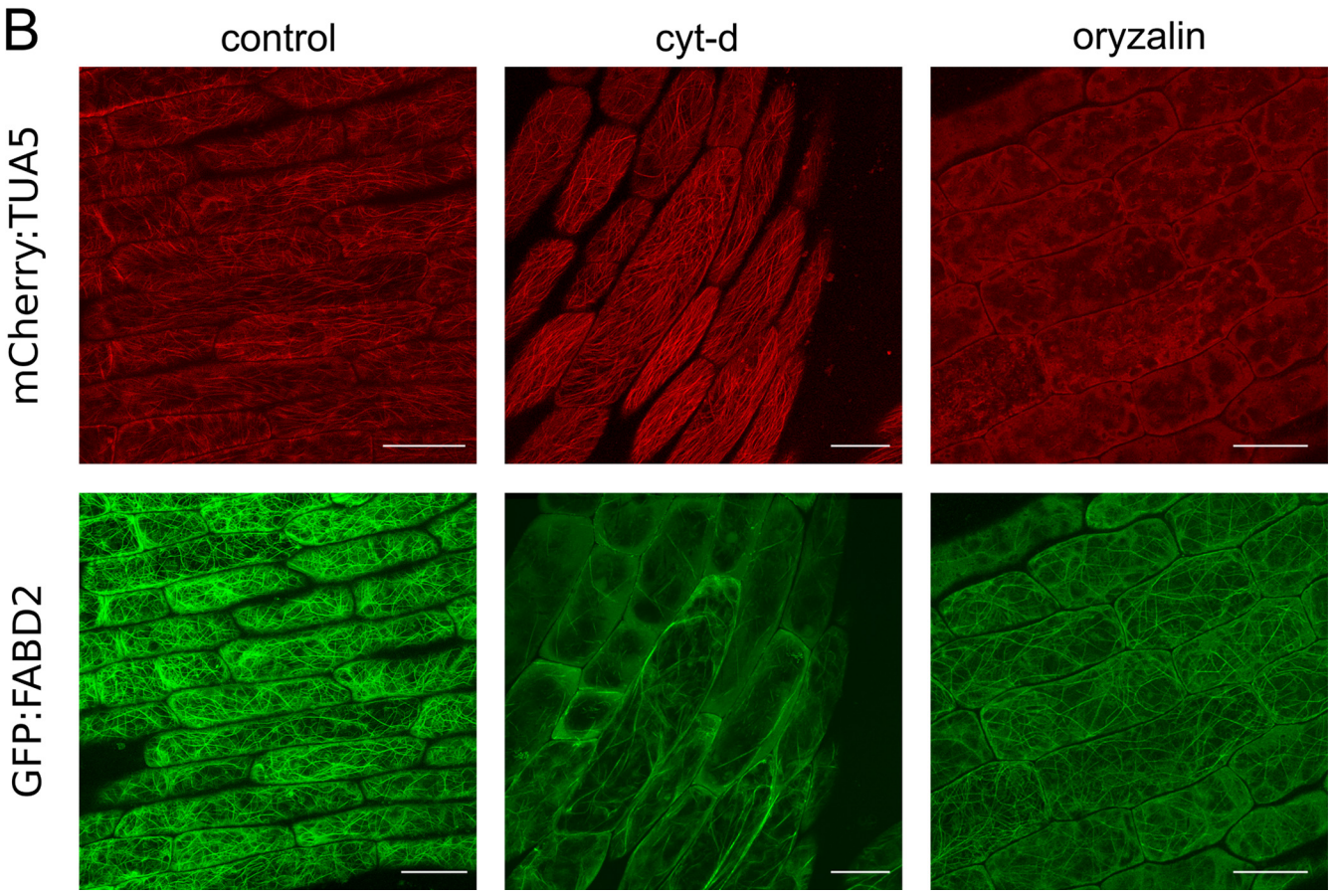
B
control
cyt-d
oryzalin
mCherry:TUA5
GFP:FABD2

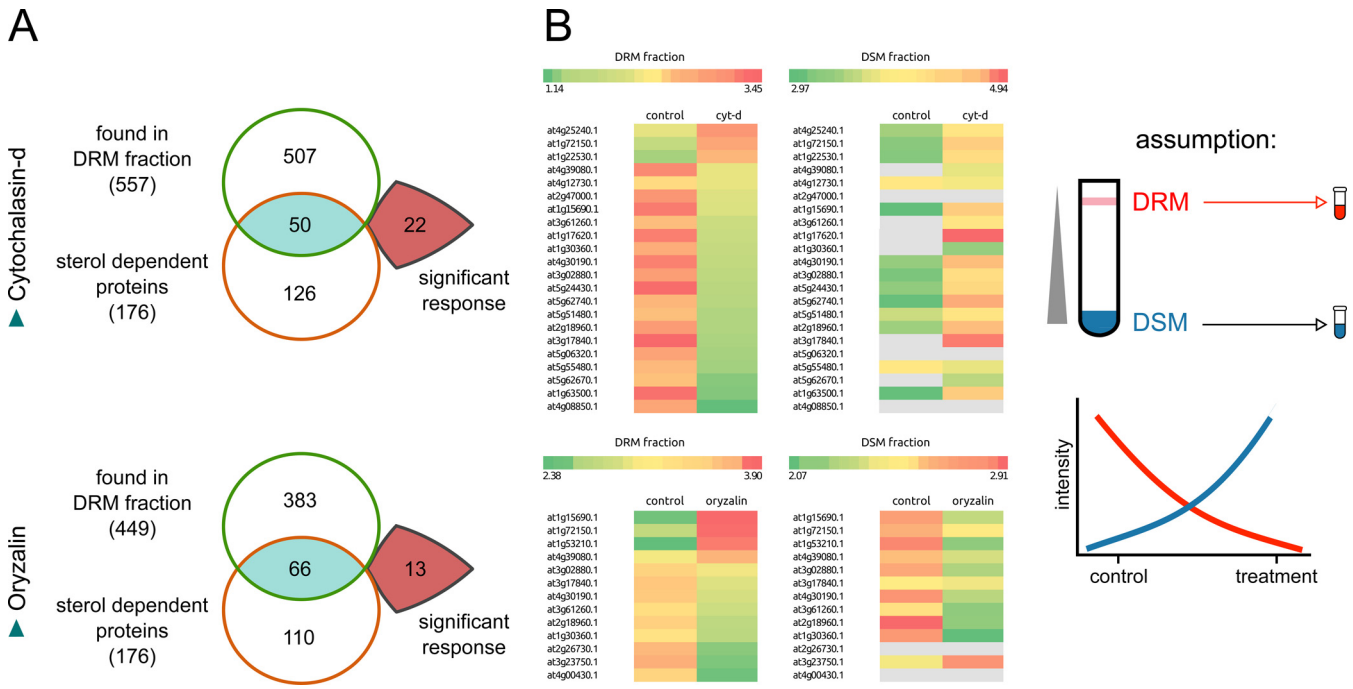

FIG. 4. (*A*) Selection of significantly responsive proteins. Candidates were selected out of the list of proteins found in DRM fraction after treatment with cytochalasin D and oryzalin that overlap with the list of sterol-dependent proteins (14) and demonstrate significant change in level in comparison to control sample (ANOVA *p* value = .05). (*B*) Expression profiles of proteins significantly responsive to cytochalasin D and oryzalin treatment. Heatmaps of average scaled intensities of treatment significantly responsive proteins. Protein abundance from DRM as well as from DSM fraction are shown for comparison.

Cytoskeletal Disruption Affects Activity of Plasma Membrane ATPase—Among the proteins with significantly altered DRM/DSM distribution profiles (Table I), we identified members of the H^+-ATPase family (AHA1, AHA2, AHA11). To study the biochemical effect of altered membrane phase recruitment, enzymatic activity assays were carried out in control and drug-treated cells. Thereby, the activity measurements of the sterol-rich DRM fractions were compared with activity measurements of total plasma membrane to relate differences in activity to differences in submembrane location (Fig. 5). Cytochalasin D treatment lead to a depletion of all three isoforms of the H^+-ATPase from the sterol-rich DRM preparations (Fig. 5*A*), and this was accompanied with an increase in the measured ATPase activity in that fraction, especially in cytochalasin D treatments of 1 h (Fig. 5*B*). Activity measured in total plasma membrane remained unaltered upon the disruption of actin filaments and was generally lower than in sterol-rich DRM fractions. These findings suggest that actin filament disruption leads to recruitment of H^+-ATPase molecules from more rigid DRM fractions to DSM (supplemental Fig. 6*A*, Table I), and this relocation is associated with an increased activity of the protein remaining in DRM. In contrast, oryzalin treatment also removed ATPase isoforms from the DRM fraction (Fig. 5*C*), but no accompanied increase in DSM was observed (supplemental Fig. 6*B*, Table I). The disruption of microtubules with oryzalin lead to a decreased H^+-ATPase activity in the DRM fraction and increased activity levels in the whole plasma membrane (Fig. 5*D*). It seems that microtubule disruption removed the plasma membrane ATPases from DRM fractions without associated relocation to DSM. In general, based on the enzyme activity measurements in combination with the resulting abundance distribution between DRM and DSM (Table I), we conclude that alterations in the location of proteins within membrane phases may signif-

Fig. 3. (*A*) Response of targeted cytoskeletal components in DRM fraction after applied treatments. Barplots represent scaled intensities of identified actin isoforms in response to (*a*) cytochalasin D and (*b*) tubulin isoforms in response to oryzalin treatment. Cytochalasin D in concentration of 500 nM for 30, 60, 90, and 120 min was applied to cell cultures. Oryzalin was applied to cell cultures for 1 h in increasing concentration range of 1 μM, 2 μM, 5 μM, and 10 μM. (*B*) Visualization of cytoskeletal components in dual-labeled *A. thaliana* seedlings. Fluorescence images of mCherry-tagged tubulin and GFP-tagged actin in the 5-day-old seedlings in response to either cytochalasin D (c = 500 nM, t = 1 h) or oryzalin treatment (c = 5 μM, t = 1 h). Recombinant proteins were expressed under the control of the ^{35}S promoter of the CM virus. Treatment with cytochalasin D causes an unaltered mCherry fluorescent signal of microtubules while fluorescent pattern of microfilaments is disturbed and equally distributed among cytoplasm. Upon treatment with oryzalin, seedlings represent an unaltered fluorescent pattern of GFP-tagged actin while signal from mCherry-tagged tubulin monomers is equally distributed among cytoplasm. Scale bars represent 20 μm.

TABLE I

Summary of proteins with increased or decreases abundance in DRM fractions upon cytoskeletal disruption with cytochalasin D or oryzalin

accession	cluster	protein name	aov p
		cytochalasin D	
at4g30190.1	1 ↓	AHA2 - H(+)-ATPase 2	5.00E-65
at1g15690.1	1 ↓	AVP1	2.05E-20
at4g39080.1	1 ↓	VHA-A3 - vacuolar proton ATPase A3	3.65E-14
at1g30360.1	1 ↓	ERD4 - Early-responsive to dehydration stress protein	7.08E-12
at3g02880.1	1 ↓	Leucine-rich repeat protein kinase	1.60E-11
at2g18960.1	1 ↓	AHA1 - H(+)-ATPase 1	2.85E-11
at1g17620.1	1 ↓	Late embryogenesis abundant hydroxyproline-rich glycoprotein	1.00E-05
at1g72150.1	3 ↑	PATL1 - PATELLIN 1	1.21E-05
at3g61260.1	1 ↓	Remorin family protein	1.57E-05
at2g47000.1	1 ↓	PGP21 - P-glycoprotein 21	2.88E-04
at5g62740.1	1 ↓	HIR1	1.27E-03
at4g25240.1	3 ↑	SKS1 - SKU5 similar 1	3.03E-03
at5g24430.1	1 ↓	Calcium-dependent protein kinase (CDPK)	3.00E-03
at4g08850.1	1 ↓	Leucine-rich repeat receptor-like protein kinase	4.22E-03
at5g62670.1	1 ↓	AHA11 - H(+)-ATPase 11	4.32E-03
at4g12730.1	1 ↓	FLA2 - FASCICLIN-like arabinogalactan 2	4.91E-03
at1g22530.1	3 ↑	PATL2 - PATELLIN 2	6.58E-03
at5g55480.1	1 ↓	SVL1 - SHV3-like 1	6.95E-03
at5g51480.1	1 ↓	SKS2 - SKU5 similar 2	0.012
at3g17840.1	1 ↓	RLK902 - receptor-like kinase 902	0.025
at5g06320.1	1 ↓	NHL3 - NDR1/HIN1-like 3	0.038
at1g63500.1	1 ↓	Protein kinase with tetratricopeptide repeat domain	0.038
		oryzalin	
at1g15690.1	3 ↑	AVP1 - Inorganic H pyrophosphatase family protein	5.73E-18
at2g18960.1	5 ↓	AHA1 - H(+)-ATPase 1	6.47E-13
at1g53210.1	3 ↑	sodium/calcium exchanger family protein	9.68E-06
at1g72150.1	1 ↑	PATL1 - PATELLIN 1	6.18E-05
at3g61260.1	5 ↓	Remorin family protein	1.87E-04
at4g39080.1	3 ↑	VHA-A3 - vacuolar proton ATPase A3	8.65E-04
at4g30190.1	5 ↓	AHA2 - H(+)-ATPase 2	9.36E-04
at3g17840.1	5 ↓	RLK902 - receptor-like kinase 902	9.68E-04
at3g02880.1	2 ↓	Leucine-rich repeat protein kinase family protein	9.96E-04
at2g21410.1	4 ↑ ↓	VHA-A2 - vacuolar proton ATPase	5.36E-03
at4g00430.1	5 ↓	PIP1;4 - plasma membrane intrinsic protein	9.31E-03
at4g30430.1	3 ↑	TET9 - tetraspanin9	0.011
at1g30360.1	5 ↓	ERD4 - Early-responsive to dehydration stress protein	0.012

icantly affect their activity either through changes in abundance or by creating activating/inactivating interaction environment.

Cytoskeletal Disruption Affects Location of a Receptor Kinase Within the Plasma Membrane—The receptor kinase AT3G02880 was found to be depleted from DRM upon treatment with cytochalasin D as well as upon treatment with oryzalin (supplemental Fig. 8*A*, Table I). The effects of drug treatment on location of AT3G02880 were analyzed using *Arabidopsis* seedlings expression a GFP-fusion under the CaMV35S promoter (supplemental Fig. 8*B*). In untreated seedlings, AT3G02880 showed more or less uniform distribution across the plasma membrane. Interestingly, the uniform distribution of fluorescent signal was exempt in line-shaped regions, resembling the cellular pattern of microtubule strands. We suggest that these exempt darker areas follow the distribution of microtubules below the membrane bilayer. This statement is supported by the finding that we did not record such distribution in oryzalin-treated seedlings, whereas it was still visible after treatment with cytochalasin D. Occasionally, locations in punctate patterns (arrows in supplemental Fig. 8*C*) were visible.

Treatment of cells with cytochalasin D did not lead to large overall changes in location pattern of AT3G02880 but enhanced the appearance of the punctate location. Treatment with oryzalin resulted in a more uniform pattern, losing the cytoskeleton negative print in the location pattern and resulting in smaller punctate structures.

Cytoskeletal Disruption Affects Location of Remorins—Remorins are plasma membrane proteins that were shown to

ASBMB MOLECULAR & CELLULAR PROTEOMICS MCP

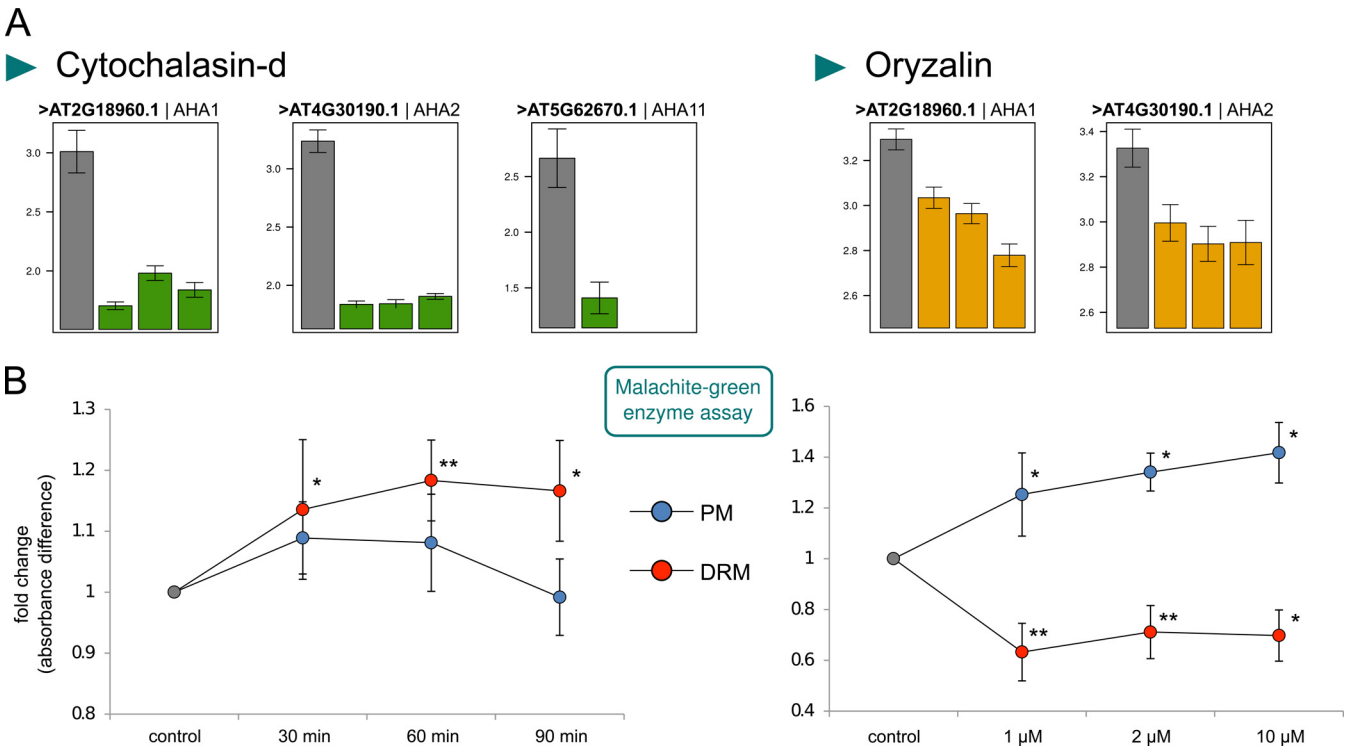

FIG. 5. **Effect of cytoskeletal disruption on plasma membrane ATPases.** (*A*) Protein abundance distribution of H+-ATPase isoforms measured by mass spectrometric analysis in response to the treatments of cytochalasin D and oryzalin. (*B*) Enzymatic measurement of ATPase activity in DRM and total plasma membrane (PM) in response to cytochalasin D and oryzalin treatment, respectively. Activity measurements were carried out with the use of malachite green enzyme assay and samples were normalized to the total protein content. Cytochalasin D in concentration of 500 nM for 30, 60, 90, and 120 min was applied to cell cultures. Oryzalin was applied to cell cultures for 1 h in increasing concentration range of 1 μM, 2 μM, 5 μ, and 10 μM.

locate to sterol-rich membrane microdomains using cell biological and biochemical approaches (9, 63), and they are highly enriched in DRM preparation (22, 60, 63). In our experiments, cytoskeletal disruptions led to altered distributions of remorin AtREM1.2 between DRM and DSM (Fig. 6*A*). These findings from the large-scale proteomic approach were confirmed by protein gel blot analysis of four fractions across the sucrose gradient separating sterol-rich DRM from sterol-depleted DSM (Fig. 6*B*). Particularly, when actin filaments were disintegrated by cytochalasin D treatment, remorin abundance clearly decreased in DRM fractions and increased in DSM. Disruption of microtubules by oryzalin also led to a depletion of remorins AtREM1.2 and AtREM1.3 from DRM, but the accompanied increase in DSM was less prominent compared with the observations in cytochalasin D treatment (Fig. 6*C*). Location of AtREM1.2 in untreated *Arabidopsis* seedlings was found in punctate patterns, as observed previously (9, 63). Treatment with cytochalasin D completely disrupted this punctate location pattern to a more uniform distribution with smaller punctate patterns of lower intensity. In contrast, treatment with oryzalin enhanced punctate location of AtREM1.2 to bigger dots of higher intensity.

DISCUSSION

This work aimed at a systematic analysis of the role of cytoskeletal components for sterol-rich membrane phase composition based on treatments with actin- or tubulin-disrupting agents. We used a proteomic screening approach to identify cytoskeleton-dependent proteins among established microdomain proteins. Enzyme assays and microscopy were then used to relate the biochemical findings to protein activities and location.

As an important prerequisite for the experimental design and the conclusions drawn, using the actin and microtubule dual-labeled line, we confirmed that the conditions used for the treatments affect only the respective cytoskeletal component and not the other. Thus, we may be able to differentiate between specific role of actin filaments or microtubules for membrane phase composition in plants.

Cytoskeleton and Protein Trafficking—All the plasma membrane constituents undergo a mechanism called secretion by which proteins, lipids, and other molecules are trafficked and delivered to their final destinations. Usual migration of proteins starts in the endoplasmic reticulum (ER) where they are synthesized. Then they are moved into the Golgi-apparatus where they obtain modifications (reviewed in (64)). Sorting of

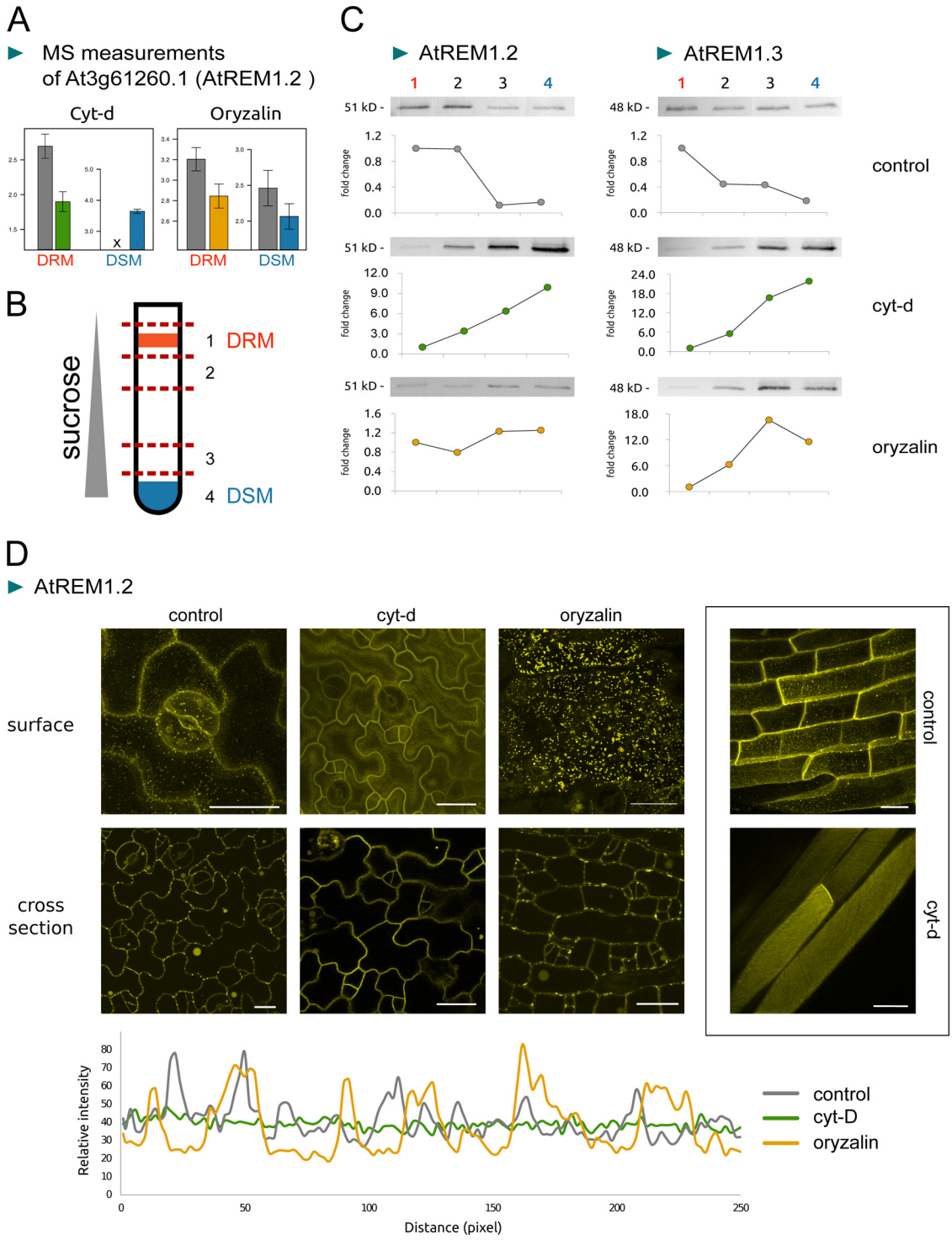

FIG. 6. **Remorins and cytoskeleton.** (*A*) Protein abundance patterns for remorin 1.2 as revealed by mass spectrometric analysis. (*B*) Schematic diagram of the sucrose gradient separating sterol-rich DRM and sterol-depleted DSF and indicated fractions sampled for analysis. Fraction 1 corresponds to the DRM fraction and fraction 4 is the DSM. (*C*) Protein gel blots of AtREM1.2 and AtREM1.3 across the fractions collected in the sucrose gradient in control samples, as well as cells treated with cytochalasin D and oryzalin. Intensity profiles are the reflections of the obtained strength of the bands' visibility (A, B, C - experiments performed on cell cultures as described in *Methods*). (*D*) Distribution of AtREM1.2:YFP under native promoter in untreated seedlings, as well as in response to cytochalasin D and oryzalin treatment. Treatment of seedlings with cytochalasin D resulted in loss of punctate location at the plasma membrane. Treatment of seedlings with oryzalin resulted in enhancement of larger punctate structures. Scale bars represent 20 μm.

proteins occurs at the trans-Golgi network from where the carriers are being transported to the targeted compartment.

It is likely that because of the close proximity, the ER and Golgi organelles do not require cytoskeletal elements to exchange carrier vesicles with each other. This was clearly proven by fluorescence recovery in the Golgi after photobleaching of fluorescent protein fusions of Golgi-localized proteins in the presence of the trafficking inhibitor brefeldin A (65, 66), in the presence of microtubule-disrupting agents (65, 66) and in cells treated with actin-disrupting agents (67). Thus, short distance membrane flow in the early secretory pathway is not impaired in the absence of functional cytoskeletal components. The secretory route from ER and trans-Golgi network to the destination membranes has not been revealed in detail. It is also unknown if trafficking to the plasma membrane is a direct process or if it includes some intermediate compartments endosomal compartments (68, 69). Although there are indications that the trans-Golgi network to plasma membrane trafficking involves exocyst complex (70), exosomes, and probably multivesicular bodies (71), it still needs to be revealed if the cytoskeleton is necessary for this process.

In contrast, participation of microtubules and actin filaments in endocytosis from the plasma membrane is quite well documented (72). Actin may create aided invaginations by specific protein–protein interactions (73–75). Importance of actin as part of the endocytotic machinery was also evaluated with the use of chemical inhibitors of actin polymerization (76). Also, microtubules were proven to play important role in both clathrin- and nonclathrin-mediated endocytosis (77).

A question that arises while analyzing the data set obtained here is whether the observed effects on the composition of detergent-resistant membrane fractions could be a result of a disturbed protein and membrane trafficking from/to the ER and Golgi apparatus. If the common trafficking pathways to the plasma membrane were disturbed, we would expect to observe some large global changes in the composition of different intracellular fractions (IM, SOL; see Fig. 1). For example, if vesicles carrying cargo destined to the plasma membrane or extracellular matrix are trapped within the cytoplasm, endoplasmic reticulum, Golgi apparatus or vacuole, a drop in protein abundance should be observed in target compartments, and an increased abundance is expected either in intracellular membrane fraction (IM) or in fraction of soluble proteins (SOL). However, the cytoskeletal disruption by cytochalasin D did not induce major global changes in protein abundances of proteins identified in the IM and SOL fractions (supplemental Fig. 5). This may indicate that observed changes in the abundance of specific proteins in the detergent-resistant membrane fraction was likely not a result of generally disturbed membrane trafficking or cell metabolism but due to rearrangements within the plasma membrane phases. Oryzalin treatment induced a large scatter of abundances of proteins identified in IM fractions, indicating a possible contribution of tubulins in protein trafficking from/to DRM fractions.

Proteins Significantly Affected by Cytoskeletal Disruption—By application of the filtering criteria, 22 proteins previously defined as sterol dependent showed a significant relocation in response to cytochalasin D and 13 proteins rearranged in response to oryzalin and nine proteins showed a significant response to both actin and microtubule disruption. These nine proteins were also previously identified as proteins with stimulus-induced abundance changes in DRM fractions either in response to flagellin (10) or during cold acclimation (78).

We observed that in response to cytochalasin D (actin filament disruption), 86% of the proteins were reduced in the DRM fraction, often displaying an associate increased abundance in the DSM fraction (Table I). In case of oryzalin treatment (microtubule disruption), a reduced abundance in DRM was observed only in 54% of the cases, and often there was no associated increase in protein abundance in DSM fractions (Table I). Thus, disruption of actin and tubulin resulted in differential distribution between the DRM and DSM fractions, although in both cases a depletion of DRM fractions was observed.

AVP1 (AT1G15690) is a type I H^+-pyrophosphatase and observed with depletion from DRM and associated enrichment in DSM in response to cytochalasin D treatment and enrichment in DRM fractions in response to oryzalin treatment. Activity of AVP1 depends on cytosolic level of potassium and is moderately sensitive to inhibition by calcium (79). Overexpression of AVP1 also enhances nutrient uptake by affecting the abundance and activity of the plasma membrane H^+-ATPase (80). Initially, AVP1 was considered to be a bona fide vacuolar marker (79, 81). However, recent studies with the use of double epifluorescence and immunogold labeling experiments showed the colocalization of AVP1 and plasma membrane located aquaporin PIP1 in plasma membrane from *Arabidopsis* (82). In the protein–protein interaction network of the proteins with altered DRM abundance upon cytoskeletal disruption, AVP1 seems to take a hub position connecting cytoskeletal elements with other ATPases such as AHA1, AHA2, AHA11, or VHA-A3 (supplemental Fig. 7).

AHA1 (AT2G18960) and AHA2 (AT4G30190) are the two most dominant plasma membrane proton pumps that generate proton gradient across the membrane in an ATP-dependent manner. Their activity results in creation of proton motive force that is used by other membrane components as a source of energy for their functions. Phosphorylation was found to be crucial mechanism for regulation of both AHA1 and AHA2 (40, 83–85). AHA1 and AHA2 were both identified as DRM constituents in several proteomic analyses (62, 78) and were additionally found as significantly enriched in DRM fractions after flg22 treatment (10). Cytoskeletal disruption lead to a depletion of AHA1 and AHA2 from DRM fractions but

ASBMB MOLECULAR & CELLULAR PROTEOMICS MCP

enzymatic assays revealed opposite effects of relocation within the membrane on H^+-ATPase activity.

Remorins—The remorin AtREM1.2 (AT3G61260) was identified as significantly responsive to actin as well as microtubule disruption. In both cases, a decreased abundance in DRM fraction was observed, but only when actin filaments were disrupted, REM1.2 showed an accompanied increased abundance in DSM. Remorins are considered as membrane microdomain markers, and they were repeatedly identified in DRM fractions by proteomic analyses (10, 22, 60, 62, 78). Immunolocalization, as well as GFP-tagging, revealed that remorins from group 1b (86) to which AtREM1.2 belongs, accumulate in distinct patches within plasma membrane. Also, in *Medicago truncatula*, MtSYMREM1 localizes in immobile domains in the plasma membrane of root hair cells (87). Here, we generally confirmed the patchy membrane location of AtREM1.2. Recent evidence, however, indicates that remorin location is quite complex and can exhibit isoform-specific patterns restricted to organs or developmental stages (9). The patchy location of AtREM1.2 in hypocotyls was abolished upon actin filament disruption, leading to uniform fluorescence with exception of the regions where microtubule strands run below the membrane bilayer.

We conclude that intact actin filaments are necessary for AtREM1.2 location to the patchy structures of membrane microdomains. Actin-dependent patchy membrane location has been described in mammalian cells also for acetylcholine receptor (in the membrane of Chinese hamster ovary that was lost when intracellular components including cytoskeleton were removed) (88).

Enhancement of patchy AtREM1.2 patterns was observed upon disruption of microtubules (Fig. 6), but the distance between the observed patches became larger. It therefore seems that disturbance of microtubules resulted in relocalization of remorin containing membrane phases or microdomains within the plasma membrane.

Contrasting Effects of Actin and Tubulin Disruption—Disruption of actin filaments or disruption of microtubules structures in many cases resulted in differential responses of the respective proteins. One general finding was that, although both drug treatments resulted in depletion of candidate proteins from DRM fractions, only for cytochalasin D treatment a respective increase in abundance of these proteins in the DSM was observed (supplemental Table 1). These observations were made initially by proteomic analysis of cell suspension cultures and then confirmed using microscopy on young seedlings. We consider the results from both systems as similar and comparable since general membrane and cytoskeleton interaction effects were studied and no specific responses in context of differentiation and cell contact. However, the cytoskeleton may be particularly important in inducing polar protein location in differentiated cells.

Treatment of the cells and seedlings with oryzalin also resulted in decreased abundance of proteins in DRM fractions, but the expected increased abundance in DSM was not measured (supplemental Table 2). These opposite effects of actin and microtubule disruption were confirmed by activity measurements for H^+-ATPase isoforms (Fig. 5), for location of receptor kinase AT3G02880 (supplemental Fig. 8), and for remorin AtREM1.2 (Fig. 6). The effects of actin disruption on remorin protein membrane location were reproduced using latrunculin B as another actin-disrupting agent (supplemental Fig. 9). Thereby, disruption of actin as well as the disappearance of the spotty localization pattern for remorin were similar as under cytochalasin D treatment.

In general, it needs to be kept in mind that the plasma membrane is a very dynamic structure. There is evidence that in plants multiple types of membrane domains with distinct composition coexist at the same time (9), and some of these could be formed in a stimulus-dependent manner or when the specific changes in lipid or protein composition occurred (87). Thus, biochemical approaches as carried out here by using changes in composition of a single biochemical fraction (here DRM) and the distribution of proteins between fractions (DRM and DSM) as readout for dynamic relocation of proteins within the membrane will not be able to distinguish these different specific microdomains observed *in vivo*. However, the approach validated identification of candidate proteins that undergo dynamic submembrane locations.

CONCLUSIONS

Various proteins found with altered distributions between DRM and DSM upon cytoskeletal disruption could be confirmed through resulting differences in activity or location patterns. Based on our results, we suggest that actin filaments are necessary for dynamic movement of proteins between different membrane phases. The effects of actin were confirmed by similar location patterns using two different actin-disrupting agents (latrunculin B and cytochalasin D). We further suggest that microtubules are not necessarily important for formation of microdomains as such, but they control the density and size of these structures (supplemental Fig. 10). Thus, if density and size of membrane microdomains changed within a cell (as, for example, observed for remorin), this could also result in an overall lower abundance of these microdomain proteins in membrane preparations and in DRM fractions. Our suggestion that microtubules may be responsible for control of size and density of membrane microdomains is further supported by the fact that more proteins with increased DRM/DSM ratio were found upon microtubule disruption treatment compared with treatment with actin-disrupting agents.

Acknowledgments—We thank Sylwia Kierszniowska for fruitful discussions on plant microdomains, Staffan Persson for supply of actin/tubulin dual-labeling lines, and Kamil Sklodowski for consultations regarding microscopy. We thank the lab of Thomas Ott (LMU Munich) for generous sharing of the remorin-GFP lines. We acknowledge the

ASBMB MOLECULAR & CELLULAR PROTEOMICS MCP

lab of Prof. Dr. Ludewig, Universität Hohenheim, for access to the confocal microscope.

* WGS was funded by the IMPRS Primary Metabolism and Growth.
S This article contains supplemental material Table 1 and Figs. 1–10.
‖ To whom correspondence should be addressed: University of Hohenheim, Department of Plant Systems Biology, 70593 Stuttgart, Germany. E-Mail: wschulze@uni-hohenheim.de.

REFERENCES

1. Singer, S. J., and Nicolson, G. L. (1972) The fluid mosaic model of the structure of cell membranes. *Science* **175,** 720–731
2. Bretscher, M. S. (1973) Membrane structures: Some general principles. *Science* **181,** 622–629
3. Baluska, F., Samaj, J., Wojtaszek, P., Volkmann, D., and Menzel, D. (2003) Cytoskeleton-plasma membrane-cell wall continuum in plants Emerging links revisited. *Plant Physiol.* **133,** 482–491
4. Simons, K., and Ikonen, E. (1997) Functional rafts in cell membranes. *Nature* **387,** 569–5672
5. Ipsen, J. H., Karlström, G., Mouritsen, O. G., Wennerström, H., and Zuckermann, M. J. (1987) Phase equilibria in the phosphatidylcholine-cholesterol system. *Biochim. Biophys. Acta* **905,** 162–172
6. Baumgart, T., Hammond, A. T., Sengupta, P., Hess, S. T., Holowka, D. A., Baird, B. A., and Webb, W. W. (2007) Large-scale fluid/fluid phase separation of proteins and lipids in giant plasma membrane vesicles. *Proc. Natl. Acad. Sci. U.S.A.* **104,** 3165–3170
7. Garcia-Sáez, A. J., Chinatia, S., and Schwille, P. (2007) Effect of line tension on the lateral organization of lipid membranes. *J. Biol. Chem.* **282,** 33537–33544
8. Malinsky, J., Operkarová, M., Grossman, G., and Tanner, W. (2013) Membrane microdomains, rafts, and detergent-resistant membranes in plants and fungi. *Annu. Rev. Plant Biol.* **64,** 501–529
9. Jarsch, I. K., Konrad, S. S., Stratil, T. F., Urbanus, S. L., Szymanski, W., Braun, F., Braun, K. H., and Ott, T. (2014) Plasma membranes are subcompartmentalized into a plethora of coexisting and diverse microdomains in *Arabidopsis* and *Nicotiana benthamiana*. *Plant Cell*
10. Keinath, N. F., Kierszniowska, S., Lorek, J., Bourdais, G., Kessler, S. A., Shimosato-Asano, H., Grossniklaus, U., Schulze, W. X., Robatzek, S., and Panstruga, R. (2010) PAMP-induced changes in plasma membrane compartmentalization reveal novel components of plant immunity. *J. Biol. Chem.* **285,** 39140–39149
11. Stanislas, T., Bouyssie, D., Rossignol, M., Vesa, S., Fromentin, J., Morel, J., Pichereaux, C., Monserrat, B., and Simon-Plas, F. (2009) Quantitative proteomics reveals a dynamic association of proteins to detergent resistant membranes upon elicitor signaling in tobacco. *Mol. Cell. Proteomics* **8,** 2186–2198
12. Roppolo, D., Boeckmann, B., Pfister, A., Boutet, E., Rubio, M. C., Denervaud-Tendon, V., Vermeer, J. E., Gheyselinck, J., Xenarios, I., and Geldner, N. (2014) Functional and evolutionary analysis of the Casparian strip membrane domain protein family. *Plant Physiol.*
13. Frescatada-Rosa, M., Stanislas, T., Backues, S. K., Reichardt, I., Men, S., Boutte, Y., Jurgens, G., Moritz, T., Bednarek, S. Y., and Grebe, M. (2014) High lipid order of Arabidopsis cell-plate membranes mediated by sterol and dynamin-related protein1A function. *Plant J. Cell Mol. Biol.*
14. Zauber, H., Burgos, A., Garapati, P., and Schulze, W. X. (2014) Plasmamembrane lipid–protein interactions affect signaling processes in sterol-biosynthesis mutants in *Arabidopsis thaliana*. *Frontiers Plant Sci.* **5,** 78
15. Demir, F., Horntrich, C., Blachutzik, J. O., Scherzer, S., Reinders, Y., Kierszniowska, S., Schulze, W. X., Harms, G. S., Hedrich, R., Geiger, D., and Kreuzer, I. (2013) Arabidopsis nanodomain-delimited ABA signaling pathway regulates the anion channel SLAH3. *Proc. Natl. Acad. Sci. U.S.A.* **110,** 8296–8301
16. Chichili, G. R., and Rodgers, W. (2009) Cytoskeleton-membrane interactions in membrane raft structure. *Cell Mol. Life Sci.* **66,** 2319–2328
17. Sako, Y., and Kusumi, A. (1994) Compartmentalized structure of the plasma membrane for receptor movements as revealed by a nanometer-level motion analysis. *J. Cell Biol.* **125,** 1251–1264
18. Oda, Y., and Fukuda, H. (2013) The dynamic interplay of plasma membrane domains and cortical microtubules in secondary cell wall patterning. *Frontiers Plant Sci.* **4,** 511
19. Ritchie, K., Iino, R., Fujiwara, T., Murase, K., and Kusumi, A. (2003) The fence and picket structure of the plasma membrane of live cells as revealed by single molecule techniques. *Mol. Membrane Biol.* **20,** 13–18
20. Shahollari, B., Peskan-Berghöfer, B., and Ölmüller, R. (2004) Receptor kinases with leucine-rich repeats are enriched in Triton X-100 insoluble plasma membrane microdomains from plants. *Physiol. Plant.* **122,** 397–403
21. Simon-Plas, F., Perraki, A., Bayer, E., Gerbeau-Pissot, P., and Mongrand, S. (2011) An update on plant membrane rafts. *Curr. Opin. Plant Biol.* **14,** 642–649
22. Kierszniowska, S., Seiwert, B., and Schulze, W. X. (2009) Definition of *Arabidopsis* sterol-rich membrane microdomains by differential treatment with methyl-β-cyclodextrin and quantitative proteomics. *Mol. Cell. Proteomics* **8,** 612–623
23. Yu, M. J., Pistikun, T., Wang, G., Anranda, J. F., Gonzales, P. A., Tchapyjnikov, D., Shen, R. F., Alonso, M. A., and Knepper, M. A. (2008) Large-scale quantitative LC-MS/MS analysis of detergent-resistant membrane proteins from rat renal collecting duct. *Am. J. Physiol.* **295,** C661–678
24. Yanagida, M., Nakayama, H., Yoshizaki, F., Fujimura, T., Takamori, K., Ogawa, H., and Iwabuchi, K. (2007) Proteomic analysis of plasma membrane lipid rafts of HL-60 cells. *Proteomics* **7,** 2398–2409
25. Nebl, T., Pestonjamasp, K. N., Leszyk, J. D., Crowley, J. L., Oh, S. W., and Luna, E. J. (2002) Proteomic analysis of a detergent-resistant membrane skeleton from neutrophil plasma membranes. *J. Biol. Chem.* **277,** 43399–43409
26. Parmryd, I., Adler, J., Patel, R., and Magee, A. I. (2003) Imaging metabolism of phosphatidylinositol 4,5-bisphosphate in T-cell GM1-enriched domains containing Ras proteins. *Exp. Cell Res.* **285,** 27–38
27. Head, B. P., Patel, H. H., Roth, D. M., Murray, F., Swaney, J. S., Niesman, I. R., Farquhar, M. G., and Insel, P. A. (2006) Microtubules and actin microfilaments regulate lipid raft/caveolae localization of adenylyl cyclase signaling components. *J. Biol. Chem.* **281,** 26391–26399
28. Donati, R. J., and Rasenick, M. M. (2005) Chronic antidepressant treatment prevents accumulation of gs-alpha in cholesterol-rich, cytoskeletal-associated, plasma membrane domains (lipid-rafts). *Neuropsychopharmacology* **30,** 1238–1245
29. Ketelaar, T., Allwood, E. G., Anthony, R., Voigt, B., Menzel, D., and Hussey, P. J. (2004) The actin-interacting protein AIP1 is essential for actin organization and plant development. *Curr. Biol.* **14,** 145–149
30. Gutierrez, R., Lindeboom, J. J., Paredez, A. R., Emons, A. M., and Ehrhardt, D. W. (2009) Arabidopsis cortical microtubules position cellulose synthase delivery to the plasma membrane and interact with cellulose synthase trafficking compartments. *Nat. Cell Biol.* **11,** 797–806
31. Pauly, M., Eberhard, S., Albersheim, P., Darvill, A., and York, W. S. (2001) Effects of the *mur1* mutation on xyloglucans produced by suspension-cultured *Arabidopsis thaliana* cells. *Planta* **214,** 67–74
32. May, J. A., Ratan, H., Glenn, J. R., Lösche, W., Spangenberg, P., and Heptinstall, S. (1998) GPIIb-IIIa antagonists cause rapid disaggregation of platelets pre-treated with cytochalasin D. Evidence that the stability of platelet aggregates depends on normal cytoskeletal assembly. *Platelets* **9,** 227–232
33. Cooper, J. A. (1987) Effects of cytochalasin and phalloidin on actin. *J. Cell Biol.* **105,** 1473–1478
34. Langhans, M., Niemes, S., Pimpl, P., and Robinson, D. G. (2009) Oryzalin bodies: In addition to its anti-microtubule properties, the dinitroaniline herbicide oryzalin causes nodulation of the endoplasmic reticulum. *Protoplasma* **236,** 73–84
35. Baskin, T. I., Beemster, G. T., Judy-March, J. E., and Marga, F. (2004) Disorganization of cortical microtubules stimulates tangential expansion and reduces the uniformity of cellulose microfibril alignment among cells in the root of *Arabidopsis*. *Plant Physiol.* **135,** 2279–2290
36. Sampathkumar, A., Lindeboom, J. J., deBolt, S., Gutierrez, R., Ehrhardt, D. W., Ketelaar, T., and Persson, S. (2011) Live cell imaging reveals structural associations between the actin and microtubule cytoskeleton in *Arabidopsis*. *Plant Cell* **23,** 2302–2313
37. Umemura, Y. M., Vrljic, M., Nishimura, S. Y., Fujiwara, T. K., Suzuki, K. G., and Kusumi, A. (2008) Both MHC class II and its GPI-anchored form undergo hop diffusion as observed by single-molecule tracking. *Biophys.*

J. **95,** 435–450
38. Collings, D. A., Wasteneys, G. O., and Williamson, R. E. (1996) Actin-microtubule interactions in the alga Nitella: Analysis of the mechanism by which microtubule depolymerization potentiates cytochalasin's effects on streaming. *Protoplasma* **191,** 178–190
39. Lanzetta, P. A., Alvarez, L. J., Reinach, P. S., and Camia, O. A. (1979) An improved assay for nanomolar amounts of inorganic phosphate. *Anal. Biochemistry* **100,** 95–97
40. Niittylä, T., Fuglsang, A. T., Palmgren, M. G., Frommer, W. B., and Schulze, W. X. (2007) Temporal analysis of sucrose-induced phosphorylation changes in plasma membrane proteins of Arabidopsis. *Mol. Cell. Proteomics* **6,** 1711–1726
41. Szymanski, W. G., Kierszniowska, S., and Schulze, W. X. (2013) Metabolic labeling and membrane fractionation for comparative proteomic analysis of *Arabidopsis thaliana* suspension cell cultures. *J. Vis. Exp.* **79,** e50535
42. Bradford, M. M. (1976) A rapid and sensitive method for the quantitation of microgram quantities of protein using the principle of protein-dye binding. *Ann. Biochemistry* **72,** 248–254
43. Rappsilber, J., Ishihama, Y., and Mann, M. (2003) Stop And Go Extraction tips for matrix-assisted laser desorption/ionization, nanoelectrospray, and LC/MS sample pretreatment in proteomics. *Anal. Chem.* **75,** 663–670
44. Cox, J., and Mann, M. (2008) MaxQuant enables high peptide identification rates, individualized p.p.b.-range mass accuracies and proteome-wide protein quantification. *Nature Biotech.* **26,** 1367–1372
45. Cox, J., Neuhauser, N., Michalski, A., Scheltema, R. A., Olsen, J. V., and Mann, M. (2011) Andromeda: A peptide search engine integrated into the MaxQuant environment. *J. Proteome Res.* **10,** 1794–1805
46. Zauber, H., and Schulze, W. X. (2012) Proteomics wants cRacker: Automated standardized data analysis of LC/MS derived proteomic data. *J. Proteome Res.* **11,** 5548–5555
47. Towbin, H., Staehelin, T., and Gordon, J. (1979) Electrophoretic transfer of proteins from polyacrylamide gels to nitrocellulose sheets: Procedure and some applications. *Proc. Natl. Acad. Sci. U.S.A.* **76,** 4350–4354
48. Bligh, E. G., and Dyer, W. J. (1959) A rapid method for total lipid extraction and purification. *Can. J. Biochem. Physiol.* **31,** 911–917
49. Lisec, J., Schauer, N., Kopka, J., Willmitzer, L., and Fernie, A. R. (2006) Gas chromatography mass spectrometry-based metabolite profiling in plants. *Nat. Protoc.* **1,** 387–396
50. Strehmel, N., Hummel, J., Erban, A., Strassburg, K., and Kopka, J. (2008) Retention index thresholds for compound matching in GC-MS metabolite profiling. *J. Chromatography B* **871,** 182–190
51. Luedemann, A., Strassburg, K., Erban, A., and Kopka, J. (2008) TagFinder for the quantitative analysis of gas chromatography-mass spectrometry (GC-MS)-based metabolic profiling experiments. *Bioinformatics* **24,** 732–737
52. Allwood, J. W., Erban, A., de Koning, S., Dunn, W. B., Luedemann, A., Lommen, A., Kay, L., Löscher, R., Kopka, J., and Goodacre, R. (2009) Inter-laboratory reproducibility of fast gas chromatography-electron impact-time of flight mass spectrometry (GC-EI-TOF/MS) based plant metabolomics. *Metabolomics* **5,** 479–496
53. Hummel, J., Strehmel, N., Selbig, J., Walther, D., and Kopka, J. (2010) Decision tree supported substructure prediction of metabolites from GC-MS profiles. *Metabolomics* **6,** 322–333
54. Kopka, J., Schauer, N., Krueger, S., Birkemeyer, C., Usadel, B., Bergmüller, E., Dörmann, P., Gibon, Y., Stitt, M., Willmitzer, L., Fernie, A. R., and Steinhauser, D. (2005) GMD@CSBDB: The Golm Metabolome Database. *Bioinformatics* **21,** 1635–1638
55. Schauer, N., Steinhauser, D., Strelkov, S., Schomburg, D., Allison, G., Moritz, T., Lundgren, K., Roessner-Tunali, U., Forbes, M. G., Willmitzer, L., Fernie, A. R., and Kopka, J. (2005) GC-MS libraries for the rapid identification of metabolites in complex biological samples. *FEBS Lett.* **579,** 1332–1337
56. Tanz, S. K., Castleden, I., Hooper, C. M., Vacher, M., Small, I., and Millar, H. A. (2013) SUBA3: a database for integrating experimentation and prediction to define the subcellular location of proteins in *Arabidopsis*. *Nucleic Acids Res.* **41,** D1185–1191
57. Thimm, O., Bläsing, O., Gibon, Y., Nagel, A., Meyer, S., Krüger, P., Selbig, J., Müller, L. A., Rhee, S. Y., and Stitt, M. (2004) MAPMAN: A user-driven tool to display genomics data sets onto diagrams of metabolic pathways and other biological processes. *Plant J.* **37,** 914–939
58. Saeed, A. I., Bhagabati, N. K., Braisted, J. C., Liang, W., Sharov, V., Howe, E. A., Li, J., Thiagarajan, M., White, J. A., and Quackenbush, J. (2006) TM4 microarray software suite. *Methods Enzymol.* **411,** 134–193
59. Saeed, A. I., Sharov, V., White, J., Li, J., Liang, W., Bhagabati, N., Braisted, J., Klapa, M., Currier, T., Thiagarajan, M., Sturn, A., Snuffin, M., Rezantsev, A., Popov, D., Ryltsov, A., Kostukovich, E., Borisovsky, I., Liu, Z., Vinsavich, A., Trush, V., and Quackenbush, J. (2003) TM4: A free, open-source system for microarray data management and analysis. *BioTechniques* **34,** 374–378
60. Zauber, H., Szymanski, W., and Schulze, W. X. (2013) Unraveling sterol-dependent membrane phenotypes by analysis of protein abundance-ratio distributions in different membrane fractions under biochemical and endogenous sterol-depletion. *Mol. Cell. Proteomics* **12,** 3732–3743
61. Benjamini, Y., and Hochberg, Y. (1995) Controlling the false discovery rate: a practical and powerful approach to multiple testing. *J. Royal Stat. Soc.* **57,** 289–300
62. Borner, G. H., Sherrier, D. J., Weimar, T., Michaelson, L. V., Hawkins, N. D., MacAskill, A., Napier, J. A., Beale, M. H., Lilley, K. S., and Dupree, P. (2005) Analysis of detergent-resistant membranes in *Arabidopsis*. Evidence for plasma membrane lipid rafts. *Plant Physiol.* **137,** 104–116
63. Raffaele, S., Bayer, E., Lafarge, D., Cluzet, S., German Retana, S., Boubekeur, T., Leborgne-Castel, N., Carde, J. P., Lherminier, J., Noirot, E., Satiat-Jeunemaître, B., Laroche-Traineau, J., Moreau, P., Ott, T., Maule, A. J., Reymond, P., Simon-Plas, F., Farmer, E. E., Bessoule, J. J., and Mongrad, S. (2009) Remorin, a Solanaceae protein resident in membrane rafts and plasmodesmata, impairs potato virus X movement. *Plant Cell* **21,** 1541–1555
64. Peer, W. A. (2011) The plant plasma membrane protein trafficking. *Plant Cell Monographs* **19,** 31–57
65. Saint-Jore, C. M., Evins, J., Batoko, H., Brandizzi, F., Moore, I., and Hawes, C. (2002) Redistribution of membrane proteins between the Golgi apparatus and endoplasmic reticulum in plants in reversible and not dependent on cytoskeletal networks. *Plant J.* **29,** 661–678
66. Brandizzi, F., Snapp, E. L., Roberts, A. G., Lippincott-Schwartz, J., and Hawes, C. (2002) Membrane protein transporter between the endoplasmic reticulum and the Golgi in tobacco leaves is energy dependent but cytoskeleton independent: Evidence from selective photobleaching. *Plant Cell* **14,** 1293–1309
67. Brandizzi, F., and Wasteneys, G. O. (2013) Cytoskeleton-dependent endomembrane organization in plant cells: An emerging role for microtubules. *Plant J.* **75,** 339–349
68. Richter, S., Voss, U., and Jürgens, G. (2009) Post-Golgi traffic in plants. *Traffic* **10,** 819–828
69. Rose, J. K., and Lee, S. J. (2010) Straying off the highway: Trafficking of secreted plant proteins and complexities in the plant cell wall proteome. *Plant Physiol.* **153,** 433–436
70. Žárský, V., Kulich, I., Fendrych, M., and Pečenková, T. (2013) Exocyst complexes multiple functions in plant cells secretory pathways. **16**
71. Ding, Y., Robinson, D. G., and Jiang, L. (2014) Unconventional protein secretion (UPS) pathways in plant. *Curr. Opin. Cell Biol.* **29,** 107–115
72. Staiger, C. J., Sheahan, M. B., Khurana, P., Wang, X., McCurdy, D. W., and Blanchoin, L. (2009) Actin filament dynamics are dominated by rapid growth and severing activity in the *Arabidopsis* cortical array. *J. Cell Biol.* **184,** 269–280
73. Samaj, J., Baluska, F., Voigt, B., Schlicht, M., Volkmann, D., and Menzel, D. (2004) Endocytosis, actin cytoskeleton, and signaling. *Plant Physiol.* **135,** 1150–1161
74. Qualmann, B., Kessels, M. M., and Kelly, R. B. (2000) Molecular links between endocytosis and the actin cytoskeleton. *J. Cell Biol.* **150,** 111–116
75. Conner, S. D., and Schmid, S. L. (2003) Regulated portals of entry into the cell. *Nature Biotech.* **26,** 1367–1372
76. Blancaflor, E. B., Wang, Y. S., and Motes, C. M. (2006) Organization and function of the actin cytoskeleton in developing root cells. *Int. Rev. Cytology* **252,** 219–264
77. Konopka, C. A., and Bednarek, S. Y. (2008) Comparison of the dynamics and functional redundancy of the *Arabidopsis* dynamin-related isoforms DRP1A and DRP1C during plant development. *Plant Physiol.* **147,** 1590–1602
78. Minami, A., Fujiwara, M., Furuto, A., Fukao, Y., Yamashita, T., Kamo, M., Kawamura, Y., and Uemura, M. (2009) Alterations in detergent-resistant

plasma membrane microdomains in Arabidopsis thaliana during cold acclimation. *Plant Cell Physiol.* **50,** 341–359
79. Maeshima, M. (1991) H+-translocating inorganic pyrophosphatases of plant vacuoles. Inhibition by Ca2+, stabilization by Mg2+ and immunological comparison with other inorganic pyrophosphatases. *Eur. J. Biochemistry* **196,** 11–17
80. Yang, H., Knapp, J., Koirala, P., Rajagopal, D., Peer, W. A., Silbart, L. K., Murphy, A., and Gaxiola, R. A. (2007) Enhanced phosphorus nutrition in monocots and dicots over-expressing a phosphorus-responsive type I H+-pyrophosphatase. *Plant Biotech. J.* **5,** 735–745
81. Maeshima, M. (2000) Vacuolar H+-pyrophosphatases. *Biochim. Biophys. Acta* **1465,** 37–51
82. Paez-Valencia, J., Patron-Soberano, A., Rodriguez-Leviz, A., Sanchez-Lares, J., Sanchez-Gomez, C., Valencia-Mayoral, P., Diaz-Rosas, G., and Gaxiola, R. (2011) Plasma membrane localization of the type I H+-PPase AVP1 in sieve elements-companion cell complexes from *Arabidopsis thaliana*. *Plant Sci.* **181,** 23–30
83. Haruta, M., Sabat, G., Stecker, K., Minkoff, B. B., and Sussman, M. R. (2014) A peptide hormone and its receptor protein kinase regulates plant cell expansion. *Science* **343,** 408–411
84. Fuglsang, A. T., Guo, Y., Cuin, T. A., Qiu, Q., Song, C., Kristiansen, K. A., Bych, K., Schulz, A., Shabala, S., Schumaker, K. S., Palmgren, M. G., and Zhu, J. K. (2007) Arabidopsis protein kinase PKS5 inhibits the plasma membrane H+-ATPase by preventing interaction with 14–3-3 protein. *Plant Cell* **19,** 1617–1634
85. Rudashevskaya, E. L., Ye, J., Jensen, O. N., Fuglsang, A. T., and Palmgren, M. G. (2012) Phosphosite mapping of P-type plasma membrane H+-ATPase in homologous and heterologous environments. *J. Biol. Chem.* **287,** 4904–4913
86. Raffaele, S., Mongrand, S., Gamas, P., Niebel, A., and Ott, T. (2007) Genome-wide annotation of remorins, a plant-specific protein family: Evolutionary and functional perspectives. *Plant Physiol.* **145,** 593–600
87. Urbanus, S. L., and Ott, T. (2012) Plasticity of plasma membrane compartmentalization during plant immune responses. *Frontiers Plant Sci.* **3,** 181
88. Kellner, R. R., Baier, C. J., Willig, K. I., Hell, S. W., and Barrantes, F. J. (2007) Nanoscale organization of nicotinic acetylcholine receptors revealed by stimulated emission depletion microscopy. *Neuroscience* **144,** 135–143

ASBMB MOLECULAR & CELLULAR PROTEOMICS MCP